View metadata, citation and similar papers at core.ac.uk

brought to you by CORE

provided by Lehigh University: Lehigh Preserve

Lehigh University
Lehigh Preserve

Theses and Dissertations

1-1-1981

Simulation of pulse response or linear distributed networks.

Joseph Cyril Gabuzda

Follow this and additional works at: http://preserve.lehigh.edu/etd


Part of the Electrical and Computer Engineering Commons

Recommended Citation

Gabuzda, Joseph Cyril, "Simulation of pulse response or linear distributed networks." (1981). *Theses and Dissertations*. Paper 2379.

This Thesis is brought to you for free and open access by Lehigh Preserve. It has been accepted for inclusion in Theses and Dissertations by an authorized administrator of Lehigh Preserve. For more information, please contact preserve@lehigh.edu.

SIMULATION OF PULSE RESPONSES OF LINEAR DISTRIBUTED NETWORKS

by

Joseph Cyril Gabuzda Jr.

A Thesis

Presented to the Graduate Committee

of Lehigh University

in Candidacy for the Degree of

Master of Science

in

Electrical Engineering

Lehigh University

1981

ProQuest Number: EP76655

All rights reserved

INFORMATION TO ALL USERS
The quality of this reproduction is dependent upon the quality of the copy submitted.

In the unlikely event that the author did not send a complete manuscript
and there are missing pages, these will be noted. Also, if material had to be removed,
a note will indicate the deletion.

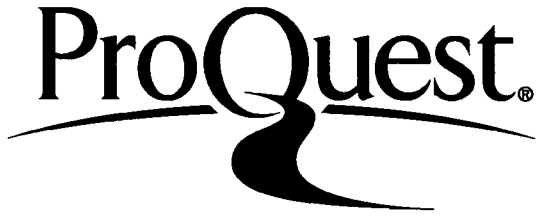

ProQuest EP76655

Published by ProQuest LLC (2015). Copyright of the Dissertation is held by the Author.

All rights reserved.
This work is protected against unauthorized copying under Title 17, United States Code
Microform Edition © ProQuest LLC.

ProQuest LLC.
789 East Eisenhower Parkway
P.O. Box 1346
Ann Arbor, MI 48106 - 1346

CERTIFICATE OF APPROVAL

This thesis is accepted and approved in partial fulfillment of the requirements for the degree of Master of Science in Electrical Engineering.

August 22 1951
(date)

Professor in Charge

Chairman of Department

Acknowledgements

I wish to thank Dr. Nikolai Eberhardt for his guidance in preparing the thesis. I also wish to thank Dr. Bruce D. Fritchman for his helpful discussions concerning the signal processing aspects. Finally, I wish to thank AMP Inc. for the loan of their equipment and use of their facilities.

TABLE OF CONTENTS

Abstract

Interconnection cables and connectors between modern fast digital circuitry often exhibit reflections due to discontinuities as well as crosstalk between adjacent lines, causing the system to malfunction. Time Domain Reflectometry can be used to detect and characterize these effects. Unfortunately, for useful interpretation of test data so far, the risetime of the test pulses had to correspond to the risetime of the digital circuitry in question.

In this paper a theoretical model is proposed and experimentally verified, that will permit to interpret data taken at fast risetimes in such a way as to predict reflections and crosstalk at any slower risetime.

The necessary mathematics is developed to allow the application of the Fast Fourier Transform algorithm to aperiodic waveforms. A computer based simulation procedure is developed. Predictions are computed from measurements made with a single 130 picosecond risetime pulse. Experimental verification is presented for both voltage reflection and crosstalk.

Wiener filtering is applied to reduce noise. The improvement after Wiener filtering is contrasted with the unfiltered signal. Finally, the industrial application of this simulation process is discussed.

1. Introduction

Modern digital circuitry contains many switching devices, the outputs of which are typically pulse trains exhibiting transitions from near zero volts to near five volts. The outputs of these switching devices are connected to a system of conductors in order to carry the signals to the inputs of other switching devices. The conductor systems are typically microstrip lines if internal to the digital system. Interconnections to other systems are typically made with flat ribbon cables. These cables are connected to the digital systems by mass termination connectors. Such a connection might include fifty different signal lines.

Solid state technological advances, such as widespread use of Schottky barrier diodes and the introduction of mid band-gap recombination sites, are causing the switching speeds of transistors to increase [12]. With the non-saturating emitter coupled logic family, switching speeds of near 400 picoseconds are available. Using the approximation that the risetime bandwidth product is .35, one finds that a 400 picosecond risetime corresponds to a 3dB bandwidth of nearly 1 gigahertz. This causes the interconnection circuitry to behave as a distributed transmission line. Discontinuities

along the line give rise to reflected waves as well as reduced transmission.

Another important aspect of the transmission line interconnection schemes is crosstalk, which can lead to false triggering of adjacent gates. The crosstalk problem is compounded now that solid state advances allow switching to occur with minimal energy, so small extraneous signals can cause false triggering.

In order to measure the voltage reflections and crosstalk in a system, Time Domain Reflectometry techniques are utilized. This basically involves exciting the system with a fast rising step of voltage and using a sampling oscilloscope to display the reflected voltages and crosstalk voltages. Because the frequency content of the voltage step is directly dependent on the risetime, and voltage reflections and crosstalk are dependent on the frequencies existing in the system, the voltage reflections and crosstalk depend on the risetime of the step.

A typical Time Domain Reflectometry unit might have a step risetime of 100 picoseconds. A manufacturer of digital interconnection systems will test a connector at this fast risetime and typically it will display severe reflections and high crosstalk levels. If a customer wishes to use this connector in a

system with a risetime of 2.75 nanoseconds, the manufacturer has no way of telling the user how the connector will perform. The manufacturers of Time Domain Reflectometry equipment have attempted to assist in this problem by making available risetime reducers which low pass filter the fast step. However, these are only available with a few selected risetimes. This places a severe limitation on the ability to specify a system's performance at nonstandard risetimes. Also, when a risetime converter is used, the typically Gaussian-shaped rise will be the signal presented in the system specifications. It would be desirable to know the interconnection system's response when excited by other waveforms. For example, the response to an exponential rise or a linear rise might be desired. Furthermore, the testing of a system with risetime converters must be done by highly trained engineers, and the Time Domain Reflectometry equipment must be available. Therefore, this project was initiated to develop a simulation procedure that would predict the voltage reflections and crosstalk at an arbitrary risetime from data taken at a fast risetime.

2. Theoretical Background

2.1 Microstrip Transmission Lines

The most common method of interconnecting digital systems is the microstrip transmission line. Microstrip is preferred because it can be batch-fabricated using standard circuit board materials and processing. Double sided circuit board material is utilized. On one side parallel conductors are formed by standard etching techniques. The other side remains a solid ground plane. A typical microstrip line is shown in Figure 1:

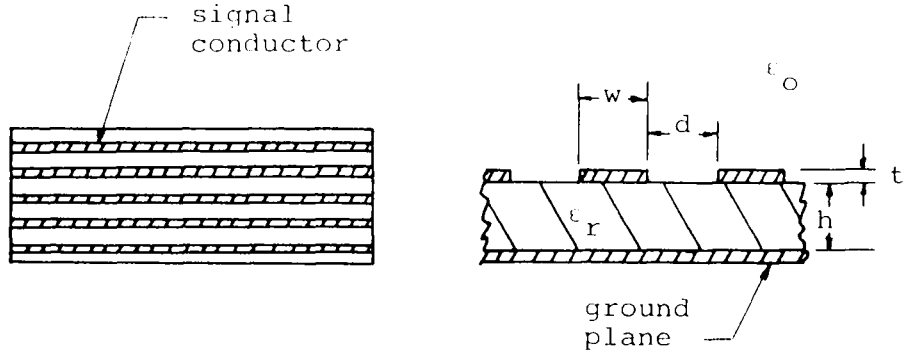

Figure 1 Typical microstrip transmission line.

Signals are introduced between the parallel conductors and the ground plane. The microstrip line driven in

this manner presents a characteristic impedance Z_c. The computation of this impedance is greatly complicated by the fact that the conductors are immersed in a mixed dielectric system. The electric field between the signal conductor and ground plane does not exist totally in the dielectric material because the width w of the signal conductor is approximately the same as the thickness of the dielectric. The characteristic impedance has been obtained by Wheeler [19] through field mapping techniques as:

$$Z_c = \frac{60}{\sqrt{.475\varepsilon_r + .67}} \ell n\left\{\frac{5.98h}{.8w + t}\right\}. \qquad (1)$$

The value of Z_c is found to be most sensitive to the ratio $\frac{w}{h}$ [5]. Standard circuit boards vary in h from .25 to 1.3 millimeters. In addition, etching considerations limit the minimum value of w to .125 millimeters. System density considerations normally limit the maximum value of w to 1.3 millimeters [8]. These factors cause the value of Z_c to be between 50 and 150 ohms. In fact, most microstrip lines used in this project had characteristic impedances of 75 ohms.

2.2 Reflections on Pulse Excited Transmission Lines

A typical microstrip system might be as indicated in Figure 2, where the resistive terminations indicate a logic gate with resistive input impedance.

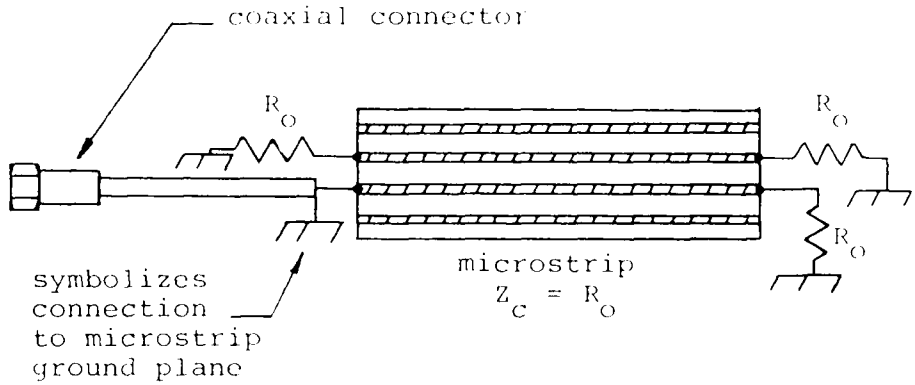

Figure 2 Idealized uniform impedance microstrip line.

The system of Figure 2 is idealized since the coaxial line has a characteristic impedance of R_o, the terminations are assumed to be resistors of value R_o, and the microstrip is assumed to have a characteristic impedance R_o. In addition, all connections are assumed to be ideal. Under these assumptions, the impedance looking into the coaxial connector will be R_o and the reflection coefficient will be zero.

In practice, such an ideal system will not exist. There can be an imperfect impedance match along a transmission line. For example, a microstrip line with characteristic impedance Z_C might be fed from a generator of impedance Z_G and terminated in impedance Z_L. The method of analysis for studying such a situation is best illustrated by an example. Consider Figure 3 where a 100 ohm source drives a length of 100 ohm line that is then connected into a terminated length of 75 ohm microstrip line.

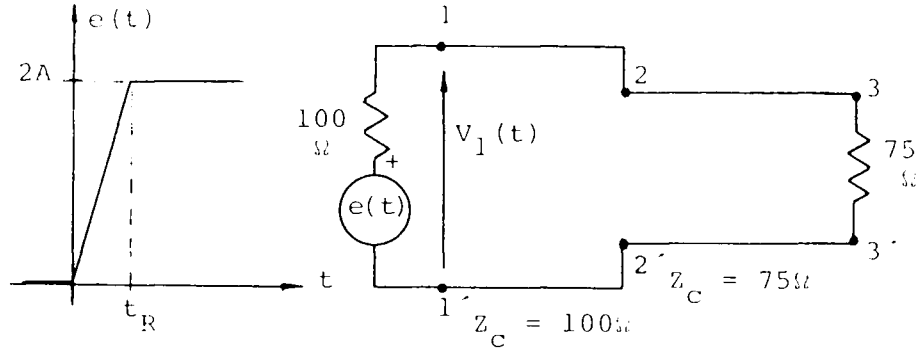

Figure 3 An impedance mismatch and assumed excitation voltage e(t).

The section of 100 ohm line is assumed to have a propagation time T_1, and the 75 ohm section a propagation time T_2. We seek to determine the voltage $V_1(t)$.

For time less than zero the voltage $V_1(t)$ is zero. For times $0 \cdot t \cdot 2T_1$, the effect of the discontinuity at terminals 2-2´will not be felt, and the voltage $V_1(t)$ is given by the voltage divider theorem as $\frac{1}{2}e(t)$. For time $t \cdot 2T_1$, the effect of the mismatch at terminals 2-2´ is felt. The reflection coefficient is given by [11]:

$$\Gamma = \frac{Z_L - Z_O}{Z_L + Z_O} = \frac{75 - 100}{75 + 100} = -.143 \quad (2)$$

The reflection coefficient is not affected by the method in which the 75Ω section is terminated, because we are considering an advancing pulse that by its causal nature cannot see what impedances lie ahead. The incident amplitude at terminals 2-2´ is A, so the reflected amplitude is -.143A. The voltage $V_1(t)$ is, as shown in Figure 4, the algebraic sum of the drive voltage and the reflected voltage.

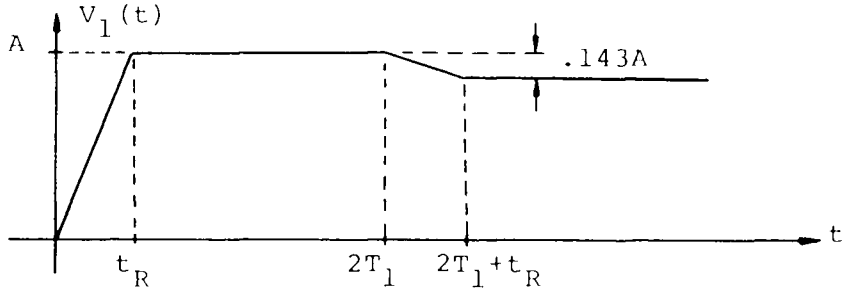

Figure 4 The resultant voltage $V_1(t)$.

The example presented was a resistive discontinuity. This can often exist in practice because of an inability to match standard ribbon cable or coaxial cable impedances to microstrip impedances.

There are frequently more complex discontinuities along digital transmission lines. These often occur when the conductor geometry is distorted, which occurs at connections and taps. A distortion of conductor geometry can result in reactive discontinuities. These may be inductive or capacitive effects, and the magnitude of the reflections is found to depend on the risetime of the digital pulses. It can be correctly concluded that any variation of uniform conductor geometry will give rise to reflections; however, it is much more difficult to predict the amplitude of these reflections.

2.3 Crosstalk Fundamentals

In addition to the problem of voltage reflections, this project will deal with crosstalk levels. While the project is concerned with predicting slower risetime crosstalk levels from measured fast risetime data, the basic theory and idealized results of crosstalk will be reviewed.

We consider a symmetrical system of parallel conductors over a ground plane and assume a mixed dielectric system. This describes a microstrip line. The two lines are schematically illustrated in Figure 5. The assumed drive line excitation $V_{in}(t)$ is also shown.

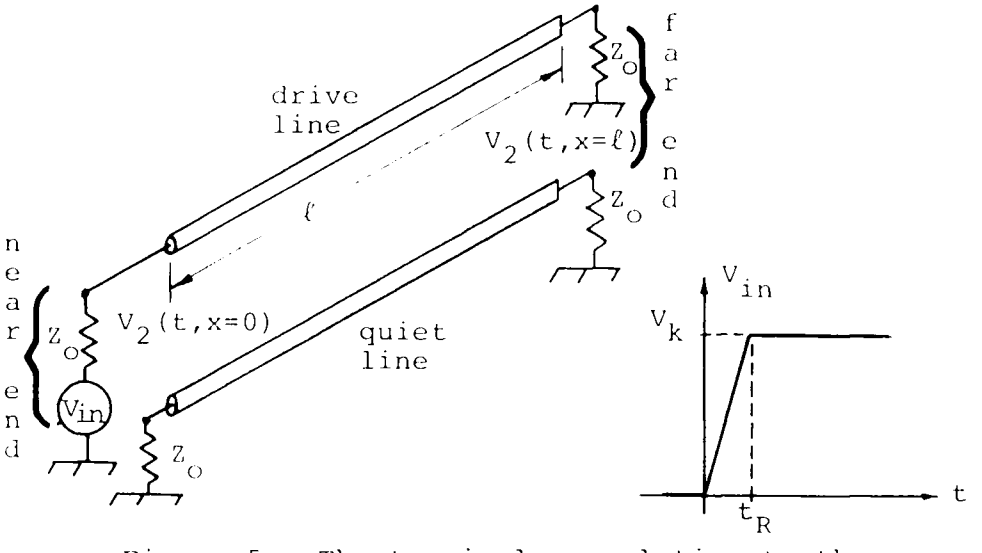

Figure 5 The terminology relating to the crosstalk problem.

Forward crosstalk is measured at the far end of the quiet line; backward crosstalk is measured at the near end of the quiet line. The drive line and quiet line are coupled via their mutual capacitance and inductance. A standard method of mathematical analysis in this type of crosstalk problem is to consider two modes existing simultaneously [2]. These modes are

properly considered to propagate independently. The two modes are termed even and odd, and are illustrated in Figure 6:

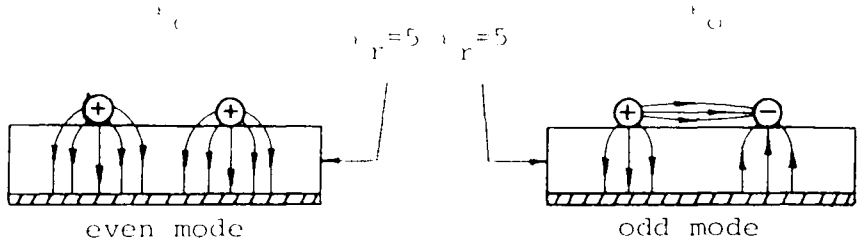

Figure 6 Mixed dielectric and two modes of propagation.

It can be visualized with the aid of Figure 6 that the odd mode propagates a larger percentage of its energy in the air than does the even mode. Therefore, the odd mode propagates faster. This effect is partially responsible for the following results.

The following results are not obvious nor intuitive. The curious reader may wish to consult several references [5,6]. A backward crosstalk pulse is theoretically predicted as indicated in Figure 7:

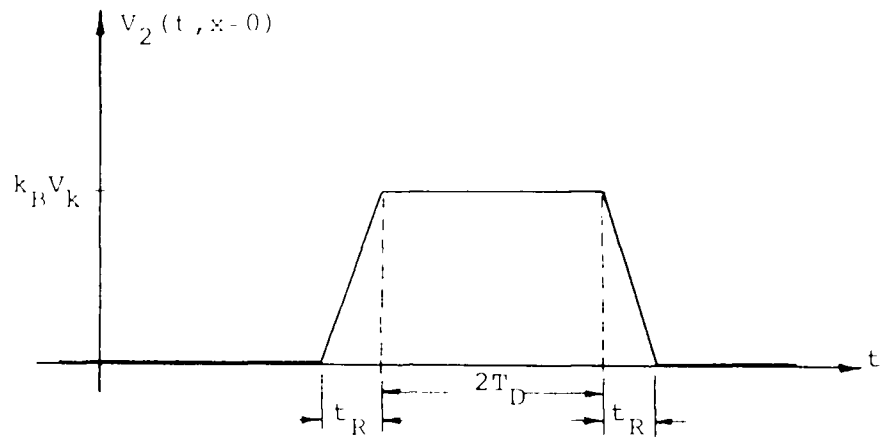

Figure 7 The back crosstalk pulse.

With reference to Figure 7, the time T_D is the propagation time for the line. Generally T_D is proportional to the line length. Providing the line is a "long line", that is the two way transit time $2T_D$ is greater than t_R, the scale factor k_B is a constant. It depends on the conductor spacing and dielectric constants, but not on the risetime t_R. In the case of a "short line", that is a line with $2T_D < t_R$, the factor k_B becomes dependent on the time derivative of $V_{in}(t)$. Finally, it is noted that the back crosstalk pulse would be present even if the dielectric surrounding the conductors were homogeneous.

We now consider the forward crosstalk at location $x = \ell$ in Figure 5. A forward crosstalk pulse is theoretically predicted as indicated in Figure 8:

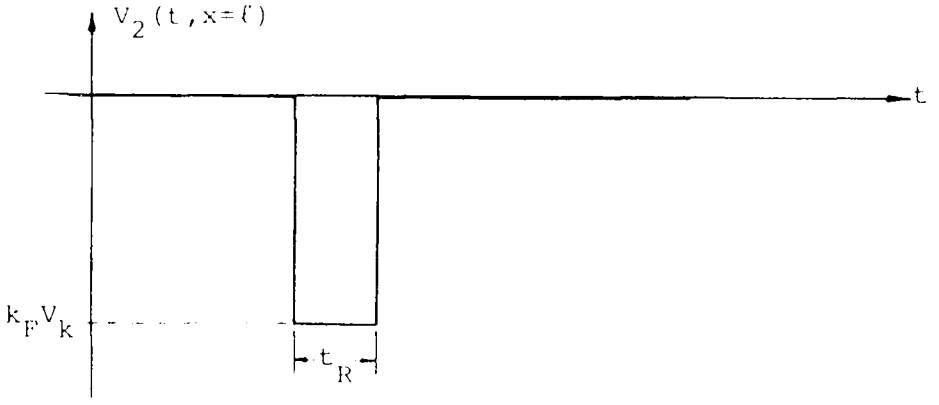

Figure 8 The theoretical forward crosstalk pulse.

The amplitude scale factor k_F is directly dependent on the risetime t_R of the drive line voltage. In addition, the pulse width is theoretically predicted to be equal to the risetime t_R. Lastly, it is pointed out that the forward crosstalk pulse would not be present if the conductors were in a homogeneous dielectric. A convenient method of demonstrating this is to take a microstrip line with epoxy based circuit board material and coat the conductors with epoxy glue. This immerses the conductors in a near homogeneous dielectric. Measurements then indicate back crosstalk

remains at the same order of magnitude, while forward crosstalk is reduced many orders of magnitude.

3. Time Domain Reflectometry

3.1 Shortcomings of Continuous Wave Testing

With the realization that various digital interconnection systems will have to be tested for voltage reflections and crosstalk level, we consider the selection of test equipment. The swept frequency method of testing involves exciting the system under test with a cw signal and using network analyzers to measure the reflected voltage. This method suffers from two shortcomings. First, the net reflected voltage is the aggregate effect of all the discontinuities along the line. This makes it impossible to determine what part of the line is causing the problem. Alternately, if there are several reflections along the line, it is impossible to assess relative severity of the discontinuities. Secondly, the swept frequency method must be extended to accumulate data at frequencies from several megahertz to several gigahertz. These data must then be mathematically processed to provide information about the system's response to pulse type waveforms.

3.2 Set-up for Voltage Reflection Measurements

A superior method of testing such digital interconnection systems is Time Domain Reflectometry (TDR). TDR is a direct method of testing in that it involves launching a step of voltage wave down the interconnection system. A block diagram of the TDR voltage reflection test set-up is given in Figure 9 [7].

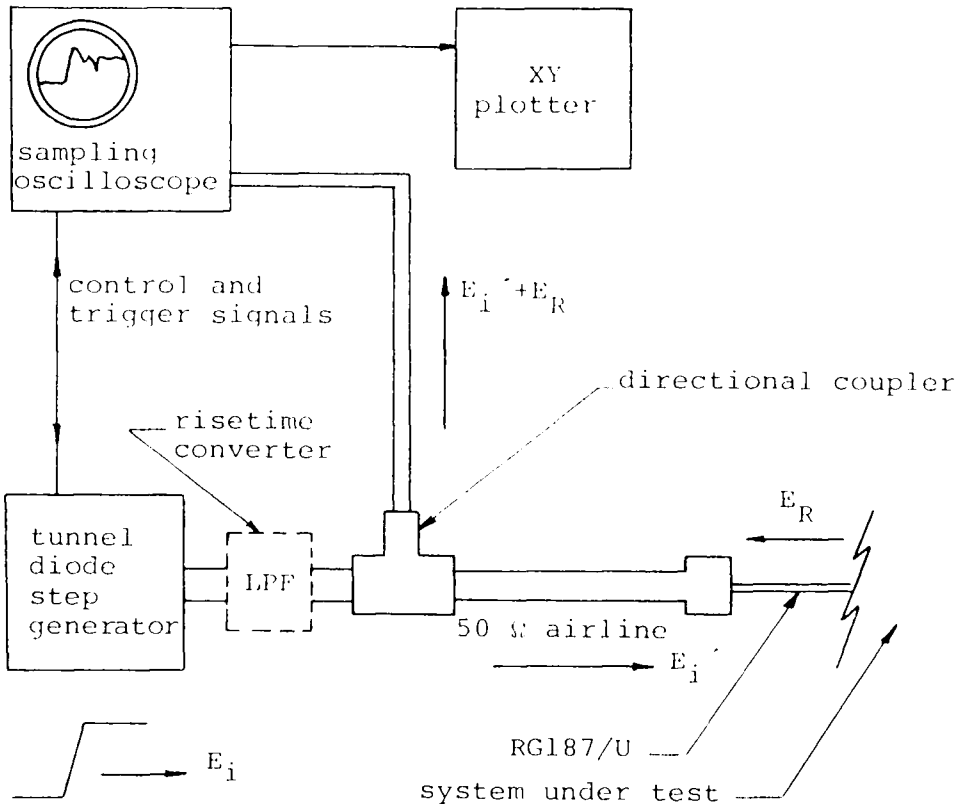

Figure 9 The TDR system set-up for reflection measurements.

A trigger circuit initiates the TDR cycle. The step generator produces a fast rising voltage step from a 50 ohm source. Following the generator is an optional low pass filter. Actually this is a rise-time converter, several of which are available, that serves to slow down the risetime of the voltage step. It is of paramount importance that the risetime at which TDR testing is done correspond to the risetime at which the system under test is to be utilized. The directional coupler [3] allows the signal E_i' to propagate down the 50 ohm airline and then down the system under test. As a result of this advancing wave, reflected voltage waves will originate at any discontinuities along the line. They will each propagate back along the system under test, through the airline, and reach the directional coupler. The directional coupler is such that it will cause the voltage wave in the line to the sampling oscilloscope to be the algebraic sum of the functions E_i' and E_R. The sampling oscilloscope takes voltage samples at discrete points along many input waveforms, and subsequently plots the results as a series of dots on the oscilloscope. Often the dot density is so high that the display is almost continuous.

The utility of this test method is that the reflected voltages isolate in time the changes in impedance along the line. The position of the reflected waveform plotted as a function of time on the display indicates the physical location of the reflection causing condition. The exact shape and amplitude of the reflected voltage can be analyzed to determine if the discontinuity is resistive, inductive, or capacitive. The relative amplitudes of all discontinuities show which must be corrected and which are acceptable[7].

3.3 Examples of Idealized Voltage Reflection Plots

Several simple examples will now serve to illustrate the TDR measurements. Consider an ideal 50 ohm line of length ℓ terminated in an open circuit. The voltage reflection coefficient ρ is defined by the ratio E_R/E_i, where E_i is the amplitude of the incident voltage wave and E_R is the amplitude of the reflected voltage wave. Considering a transmission line of characteristic impedance Z_o terminated in a load Z_L, the reflection coefficeint ρ is given by [11]

$$\rho = \frac{Z_L - Z_o}{Z_L + Z_o} \quad . \qquad (3)$$

In the case of an open circuit termination, Equation (3)predicts that ρ equals +1. Therefore, the reflected

waveform is equal in amplitude to the incident waveform, and of the same polarity. The reflected waveform will reach the directional coupler after a delay time equal to the transit time down and back the line under test. The one way transit time is termed T_D. The resultant voltage reaching the oscilloscope is therefore given in Figure 10.

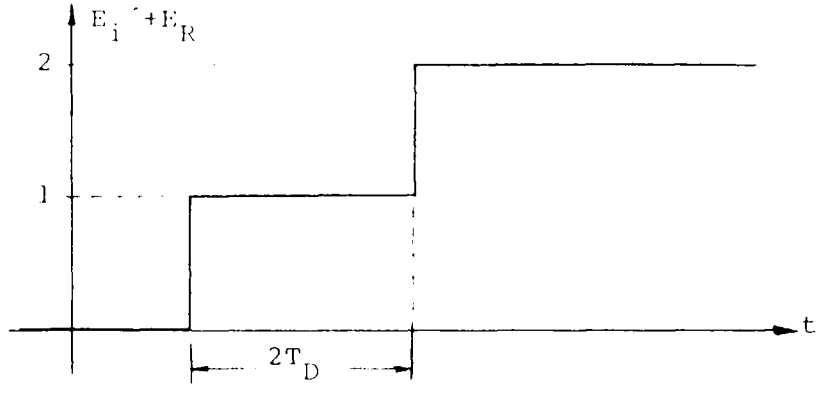

Figure 10 Idealized TDR plot for an open-circuited line.

If the line had been terminated in a short, similar anaylsis would have given a voltage plot as shown in Figure 11:

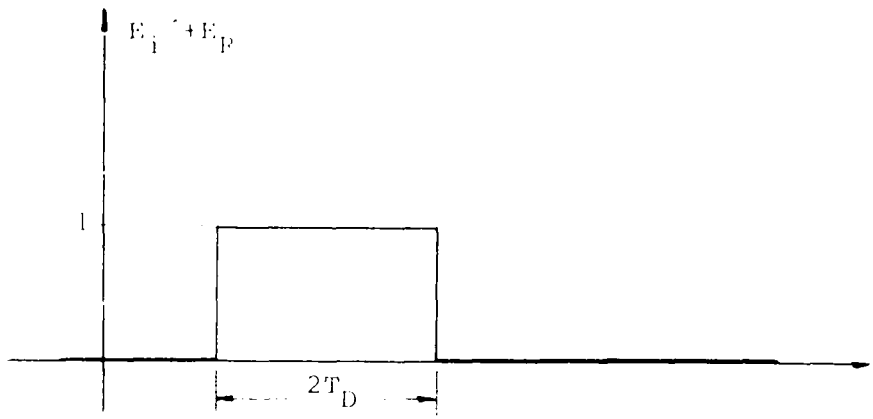

Figure 11 Idealized TDR plot for a shorted line.

It is also instructive to consider a uniform 50 ohm line terminated in a capacitor C_L. As with other terminations, we will just see the excitation voltage step existing for time $2T_D$. Following time $2T_D$, we will see the sum of the incident step and the reflected voltage. When the incident pulse initially reaches the capacitor, it will behave as a short circuit. After the capacitor charges, it will present an open circuit. The transition will be exponential [18] with a time constant $\tau = 50\Omega \cdot C_L$. Recalling Figures 10 and 11, we can construct the TDR plot for the capacitive load. In a like manner, the TDR voltage reflection plot for an inductive load L can be determined.

These are presented in Figure 12:

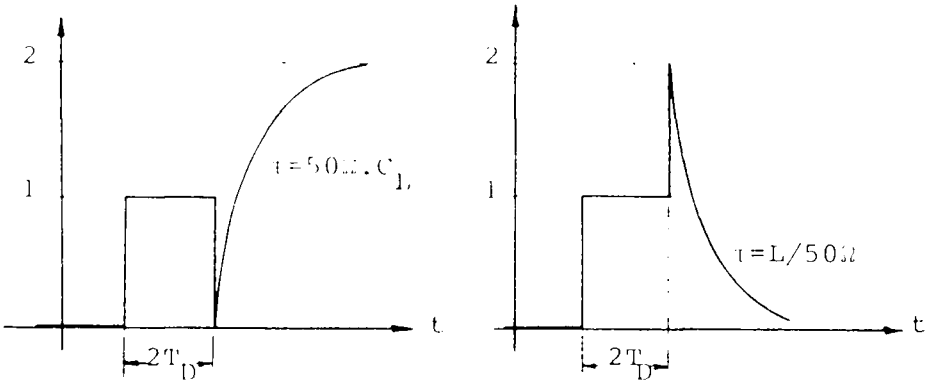

Figure 12 TDR voltage reflection plots for capacitive and inductive loads.

In practice, the occurrence of spikes like those in Figure 12 is common. The direction (up or down) is used to determine if the discontinuity is largely inductive or capacitive.

3.4 Set-up for Crosstalk Measurements

In addition to voltage reflection studies, the TDR equipment can also be used to measure crosstalk. The equipment must be connected differently, and details of this are indicated in Figure 13.

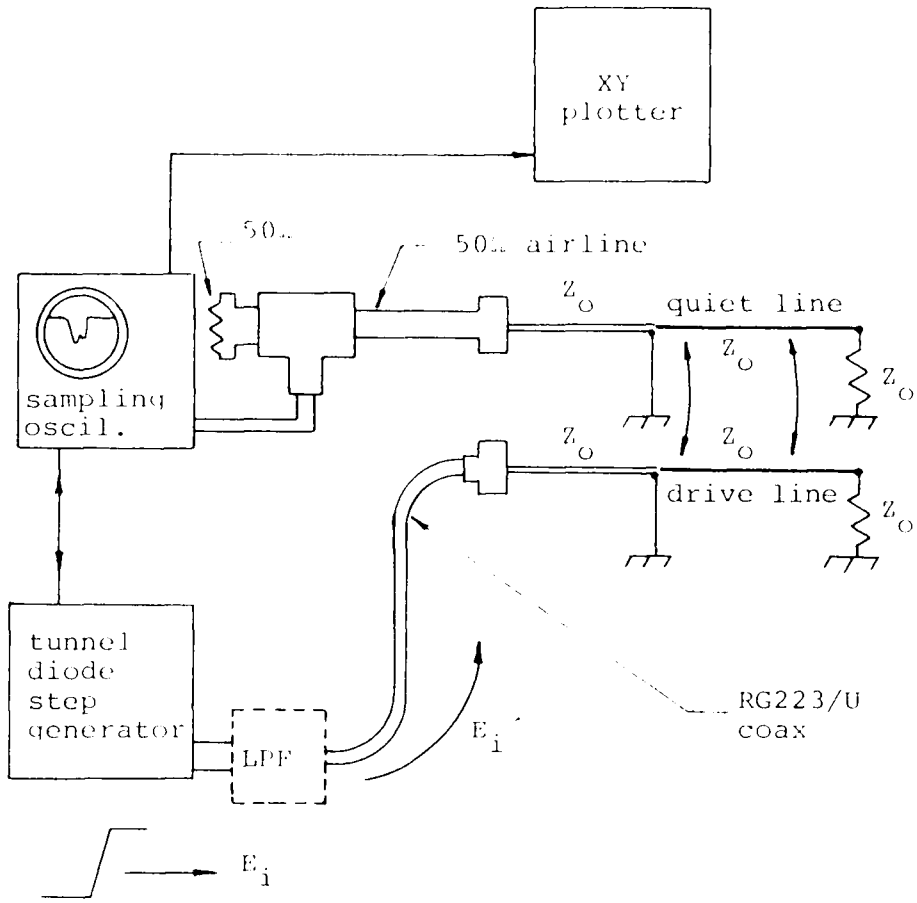

Figure 13 Crosstalk measurement with TDR equipment.

The tunnel diode pulse generator is used to apply the voltage drive to the drive line. The optional rise-time converter can be installed to slow down the voltage step. One leg of the directional coupler is terminated in its characteristic impedance (50Ω), so

the sampling oscilloscope will record just the voltage on the quiet line. As illustrated, the system measures back crosstalk; forward crosstalk is measured by placing the sampling oscilloscope pick-up at the far end and the termination Z_o at the near end of the quiet line.

It should be noted that if the system under test has a characteristic impedance Z_o, and Z_o is not 50 ohms, the crosstalk pulses will experience reflection at the junction from the quiet line to the 50 ohm airline. This reflection is important if the actual amplitude of the crosstalk pulses is needed. If this is needed, one can apply a mathematical correction factor. Alternatively, it may be more accurate to proceed as follows: connect the 50 ohm airline and quiet line system into a TDR voltage reflection set-up. This will result in an oscilloscope display of the 50 ohm level and a different level corresponding to the Z_o impedance level. Next, note the amplitude of the Z_o level and adjust the vertical vernier so the 50 ohm level assumes this amplitude. Now the TDR unit may be used for crosstalk measurements and no further correction is necessary.

4. Theory and Computer Simulation

4.1 Preliminary Investigations

Consider an arbitrary transmission system, that is one that might include sections of microstrip, coaxial line, and connectors. There will, in general, be a linear dielectric material separating the conductors. Epoxy based circuit board material is predominant in a microstrip system; various plastics are used in connectors. Regardless of the conductor geometry, the fields will be described by solutions of Maxwell's curl and divergence equations. In linear media, these equations have the property that solutions remain solutions under linear operations. Therefore, it should be possible to consider the overall transmission system from the standpoint of linear system analysis. The standard method of linear system analysis is illustrated in Figure 14:

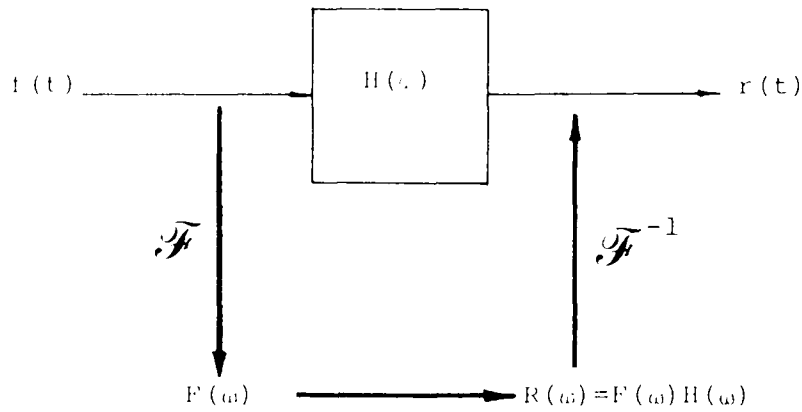

Figure 14 The notation of linear system analysis.

A two port linear system with transfer function $H(\omega)$ is shown with input signal f(t). The symbol $\mathcal{F}$ denotes Fourier transformation; $\mathcal{F}^{-1}$ denotes an inverse Fourier transformation. The heavy line weight arrows indicate the steps involved in the frequency domain approach to calculating r(t). The transfer function $H(\omega)$ can be found from the ratio of the Fourier transforms of an arbitrary excitation function and corresponding response.

The method of linear system anaylsis is applied to the TDR testing problem by considering the input port to be at the location of E_i' in Figure 9. The

output port is taken to be the oscilloscope screen. The input function corresponding to f(t) in Figure 14 is taken to be $E_i'(t)$; the output function, corresponding to r(t), is taken to be the oscilloscope trace. The oscilloscope trace can be recorded on any X-Y plotter.

An example of the application of linear analysis to TDR is now presented. The considered circuit may be representative of a real situation [16]. Additionally, it will give the reader a better feeling for the novel analysis that lies ahead.

Consider a uniform 50 ohm coaxial line terminated in a capacitive load C_L. Details are given in Figure 15:

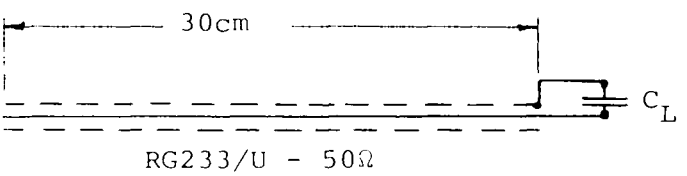

Figure 15 The capacitively loaded transmission line.

The TDR transfer function for this system can be obtained in closed form by a simple argument. Envision the previous system to be installed in a TDR system that has an ideal step of voltage as the excitation function. The TDR voltage reflection response of a capacitively loaded line when excited by an ideal step was given in Figure 12, and is repeated here for convenience:

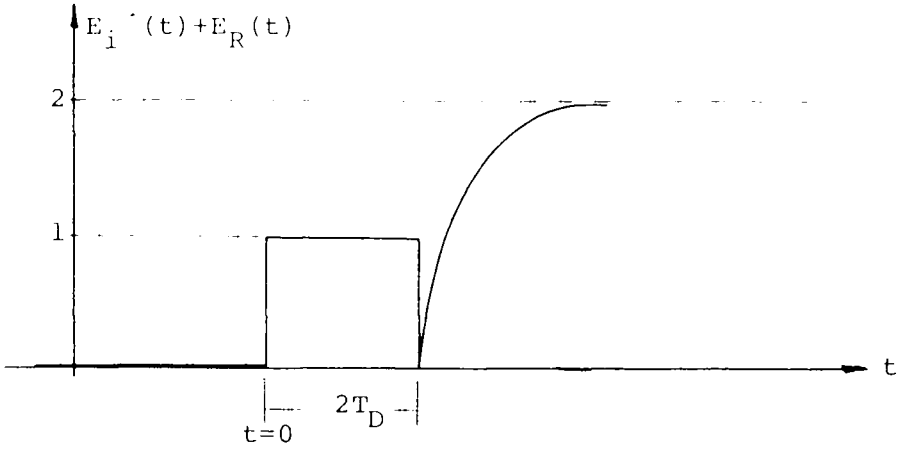

Figure 16 The idealized TDR voltage reflection plot from the system of Figure 15.

Next, by defining $r(t) = E_i'(t) + E_R(t)$, we can express $r(t)$ as:

$$r(t) = u(t) - u(t-2T_D) + 2(1-e^{-(t-2T_D)/\tau_L})u(t-2T_D) \quad . \qquad (4)$$

The Laplace transform of r(t) is found to be

$$R(s) = 1/s(1-e^{-2T_D s}) + \frac{2e^{-2T_D s}}{s}\left(\frac{1}{1+s\tau_L}\right). \quad (5)$$

The Laplace transform of the input $E_i'(t)$, which was assumed to be u(t), is given by

$$E_i'(s) = \frac{1}{s}. \quad (6)$$

The TDR transfer function is obtained by division of R(s) by $E_i'(s)$, which yields

$$H(s) = 1 - e^{-2T_D s} + 2e^{-2T_D s}\left\{\frac{1}{1 + s\tau_L}\right\}. \quad (7)$$

Notice H(s) has been obtained effectively by inspection of the system. Remembering that this present problem is an idealized situation in which the transfer function was obtained in a closed form, we will make another assumption. We assume the slower steps (as will be provided by the risetime converters) can be approximated by exponentials. This is not the best approximating function, as can be seen in Appendix 1. However, the exponential function will make the mathematics tractable. Therefore, the slower input steps are assumed to be of the form

$$E_{i,\tau}' = (1-e^{-t/\tau})u(t). \quad (8)$$

The response to these slower steps has been derived using standard linear system analysis. The mathematics is lengthy; therefore, the analysis is presented in Appendix 2. The response to a step of the form of Equation (8) is found to be

$$r(t) = (1-e^{-t/\tau})u(t) + \left\{ 1 + \left(\frac{2}{\frac{\tau}{C_L Z_o} - 1}\right) \cdot e^{-(t-2T_D)/C_L Z_o} + \frac{\tau + C_L Z_o}{C_L Z_o - \tau} \cdot e^{-(t-2T_D)/\tau} \right\} u(t-2T_D). \quad (9)$$

where τ is the all important risetime parameter. Typical plots of this response are given in Figure 17:

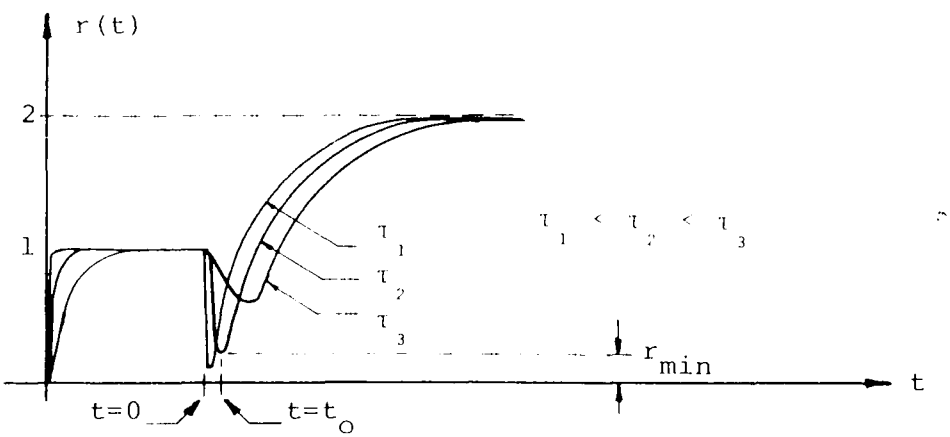

Figure 17 Predicted TDR plots for the system of Figure 15 tested by a slower than ideal step of voltage.

Equation (9) predicts a changing response as τ varies. In the limiting case that τ tends to zero, Equation (9) predicts the same response as shown in Figure 16. As τ increases, Equation (9) predicts an increasing value of t_o and increasing value of r_{min}.

At this point we have arrived at a closed form expression for the response through the use of a TDR transfer function. To test the validity of the predictions, the transmission system illustrated in Figure 15 was connected into the TDR system and the response to various speed steps was recorded. Specifically, risetimes of 130 picoseconds, .5 nanosecond, 1 nanosecond, 2 nanoseconds, and 5 nanoseconds were used. The 130 picosecond step is the unslowed output from the HP 1415A TDR unit. The slower risetimes were obtained by installing Hewlett Packard risetime converters.

With data collected at 5 risetimes, Equation (9) will be used to make corresponding predictions. Because of the characteristics of an exponential rise, a least squares analysis indicates that defining risetime from 20 percent to 80 percent points is better than from 10 percent to 90 percent points. Using this assumption, it can be shown that the relationship

between t_R and τ is given by:

$$t_R = 1.39\tau \,. \tag{10}$$

This equation is used in preparing Table 1. The most interesting aspect is the value of e_{min}. The minimum point e_{min} can be determined from Equation (9) by differentiation, resulting in

$$e_{min} = 2 + \frac{2\,C_L Z_o}{\tau - C_L Z_o} \cdot \left[\frac{2\tau}{\tau + C_L Z_o}\right]^{-\frac{\tau}{\tau - C_L Z_o}} + \frac{\tau + C_L Z_o}{C_L Z_o - \tau} \cdot \left[\frac{2\tau}{\tau + C_L Z_o}\right]^{-\frac{C_L Z_o}{\tau - C_L Z_o}} . \tag{11}$$

The comparison between measured data and predicted data is now made. These results are given in Table 1.

TABLE 1

Experiment Risetime	Experimental Value E_{min}	Prediction Time Constant (per (10))	Predicted Value e_{min} (per (11))
130 psec	.2	93.5 psec	.12
.5 nsec	.3	.36 nsec	.29
1 nsec	.4	.719 nsec	.42
2 nsec	.58	1.44 nsec	.56
5 nsec	.75	3.6 nsec	.74

The agreement is good. In addition, comparison of the complete plots of experimental and predicted responses was made and good agreement found.

The results of this example have given great support to the use of a transfer function approach. This approach must now be extended to cases where the transfer function must be obtained from samples of the fast input step and corresponding response. In addition, the transforms of the slower input steps will come from sampled signals.

4.2 Modification of Discrete Fourier Transform

Since we will be attempting to form the Fourier transform of a sampled signal, the discrete Fourier transform (DFT) will be employed. Numerous authors develop [1] and discuss [15] the DFT. Here the essential aspects are repeated. Given a bandlimited periodic signal f(t) with period T and positive frequency bandwidth w, it can be exactly represented by sampling at the Nyquist rate $\omega_s = 2w$. Assuming there are N samples, N being given by the ratio of ω_s to $\omega_o = 2\pi/T$, we have a sampled data array

$$f(n) = f(n \frac{2\pi}{\omega_s}) \qquad n = 0,1,2,\ldots,N-1. \qquad (12)$$

Now N DFT coefficients (N/2 being unique for real f(n)) can be obtained from

$$F(k) = \frac{1}{N} \sum_{n=0}^{N-1} f(n) W^{+nk} \qquad (13)$$

where $W = e^{-j2\pi/N}$. The N DFT coefficients F(k) correspond to frequencies $k\omega_0$. In addition, if sampling is done at or above the Nyquist rate, the DFT coefficients F(k) will equal the true Fourier coefficients of f(t).

Realizing that most TDR waveforms are step-like, the DFT will have to be modified. A step-like waveform starts at zero, undergoes a transient excursion to a new constant level A, and remains there for a long time. This is illustrated in Figure 18:

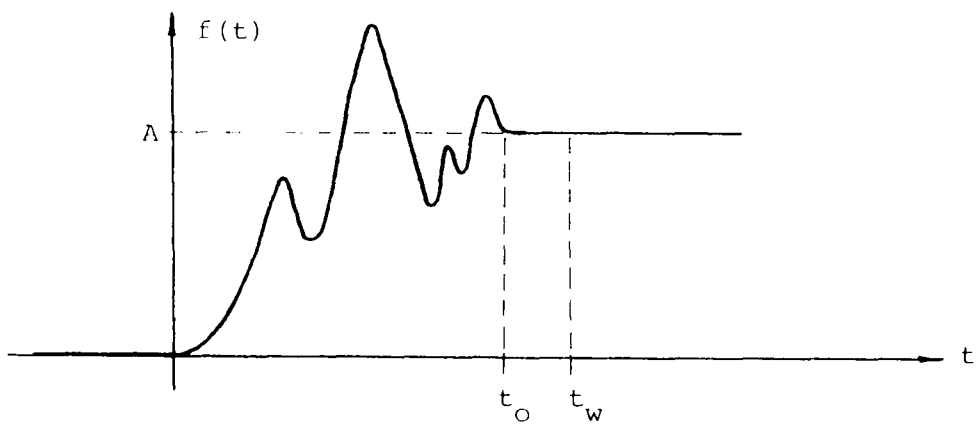

Figure 18 This illustrates a step-like waveform.

Note the waveform is aperiodic. If one attempts to apply the standard DFT to f(t), a rectangular window is applied to determine the interval over which samples are taken. As a practical matter, if one is to obtain a sufficient number of samples of f(t) in the region $[o,t_o]$ so the Nquist condition is realized or aliasing [14] is at a tolerable level, it is impossible to extend the window much beyond $[o,t_o]$. Assuming one chooses a window $[o,t_w]$, the standard DFT algorithm will be assuming the signal is periodic, and the signal that gets transformed is shown in Figure 19:

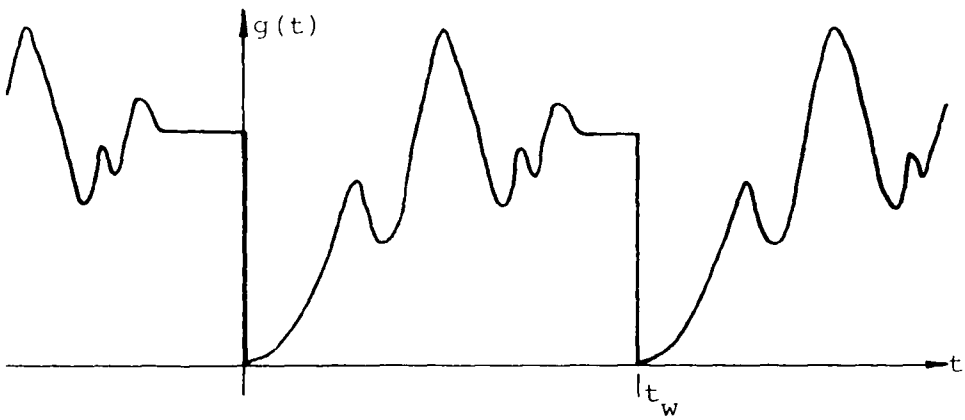

Figure 19 The standard DFT assumes periodicity of the sampled signal.

Clearly the spectrum of g(t) will contain many high frequency components due to the step transition at t_w. These high frequency components mask the much

smaller corresponding components in the spectrum of f(t). This problem is predicted [1] and was experimentally verified. The resolution of this problem was an extremely important step in the project; therefore, it will be discussed in detail. Initially the discussion will deal with the Fourier transform. The extension to the DFT follows.

Consider attempting to form the Fourier transform of f(t) as depicted in Figure 18. This transform is given by an integration over the infinite domain $(0,\infty)$ as

$$F(\omega) = \int_0^{\infty} f(t)^{-j\omega t} dt \qquad (14)$$

However, it is possible to obtain a large number of values of $F(\omega)$ by integration over the finite domain $[o,t_w]$. Consider the following auxiliary function r(t), depicted in Figure 20:

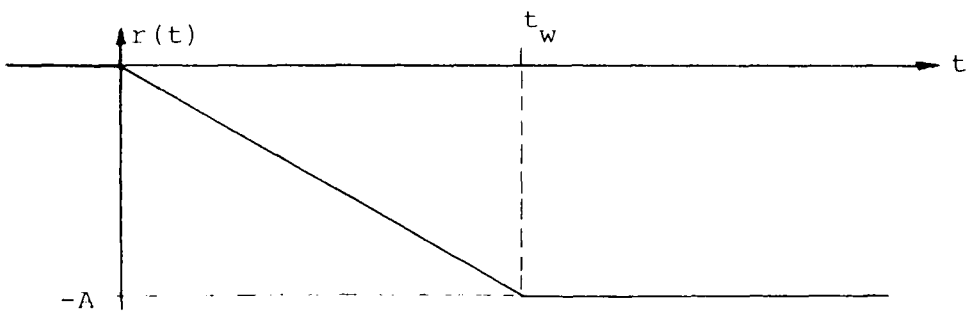

Figure 20 The ramp function r(t) serves an auxiliary role. The level "A" corresponds to that of Figure 18.

The Fourier trnasform of r(t) is obtained as

$$R(\omega) = \begin{cases} \dfrac{-2Ae^{-j\omega t_w/2}}{j\, t_w \omega^2} \sin \dfrac{\omega t_w}{2} & \omega \neq 0 \\ -A\pi\delta(\omega) & \text{all } \omega \end{cases} \qquad (15)$$

Next, form the sum of f(t) (from Figure 18) and r(t). This result is sketched in Figure 21.

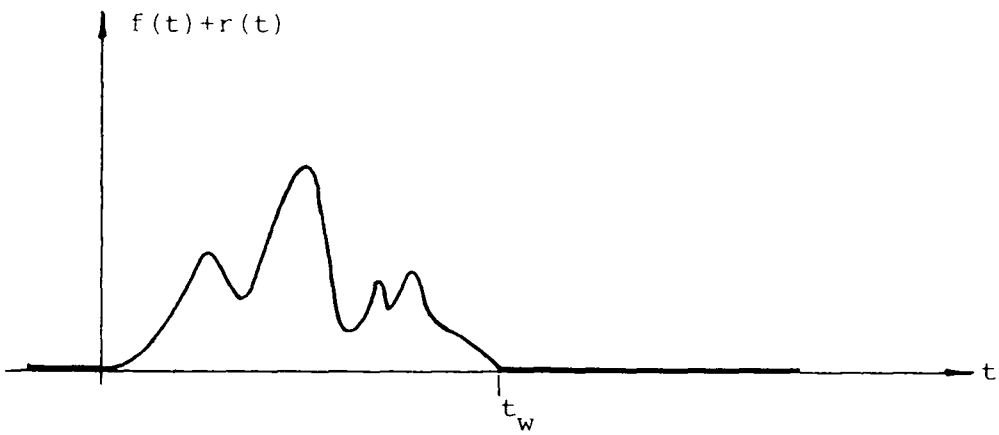

Figure 21 This illustrates the sum f(t) + r(t) is nonzero only over the region $[o,t_w]$.

The key point is that f(t) + r(t) is no longer a step-like waveform, but has its nonzero values limited to a finite domain $[o,t_w]$. Therefore, the Fourier transform of f(t) + r(t) can be obtained by an integration over a finite domain as:

$$F(\omega) + R(\omega) = \int_0^{t_w} [f(t)+r(t)]\, e^{-j\omega t} dt \qquad (16)$$

Now the crucial step is to notice that $R(\omega)$, as given in Equation (15), is zero for nonzero frequencies $k\omega_o$, where $\omega_o = 2\pi/t_w$. Therefore, the values of $F(\omega)$ in Equation (14) for $\omega = k\omega_o$ $(k \neq 0)$ can be obtained from the finite integration in Equation (16). The uncertainty of the DC term $F(0)$ will not be a problem. Also, we must recognize that in actuality the signal $f(t)$ contains frequency components at all frequencies. The above procedure allows one to obtain samples of the continuous transform.

The above technique of adding in a ramp to force the sum $f(t) + r(t)$ to be zero at the endpoints 0 and t_w will allow the application of the DFT without any truncation error [13,17]. Since we will be adding $f(t)$ to $r(t)$, the DFT of the sum will be the sum of the corresponding DFT's. Assuming sampling is done at the Nyquist rate, the DFT coefficients will equal the Fourier coefficients, and the above argument concerning frequencies $k\omega_o$ applies. Taking N samples of $r(t)$ in the interval $[o,t_w]$ gives the samples

$$r(n) = \frac{-An}{N} \qquad (17)$$

The N DFT coefficients can be obtained from

$$R(k) = \frac{1}{N} \sum_{n=0}^{N-1} \frac{-An}{N} e^{-j \frac{2\pi nk}{N}} . \quad (18)$$

This finite summation requires substantial effort to evaluate, and the result cannot be found in most tables, so it is presented here. First we introduce

$$W = e^{-j\ 2\pi k/N} \quad (19)$$

and upon forming an auxiliary function

$$H(k) = R(k) - WR(k) \quad (20)$$

we find

$$H(k) = \frac{-A}{N^2} \left[\sum_{n=0}^{N-1} nW^n - \sum_{n=0}^{N-1} nW^{n+1} \right] . \quad (21)$$

Index manipulation easily yields

$$H(k) = \frac{-A}{N^2} \left[\sum_{n=1}^{N} nW^n - NW^N - \sum_{n=1}^{N} (n-1)W^n \right] . \quad (22)$$

Collecting terms under a common summation yields

$$H(k) = \frac{-A}{N^2} \left[\sum_{n=1}^{N} W^n - NW^N \right] . \quad (23)$$

Next, we examine the summation Equation (23) by using the relation

$$\sum_{n=0}^{N-1} X^n = \frac{1 - X^N}{1 - X} \qquad \text{all } X. \tag{24}$$

Since we know $W^0 = W^N$ from Equation (19), the summation in Equation (23) is

$$\sum_{n=1}^{N} W^n = \sum_{n=0}^{N-1} W^n . \tag{25}$$

Now, using Equation (24) on the right side of Equation (25) gives

$$\sum_{n=0}^{N-1} W^n = \frac{1 - W^N}{1 - W} = 0 \qquad k \neq 0 \tag{26}$$

since $W^N = 1$ from Equation (19). Now the result emerges from Equations (20), (23), and (26) as

$$H(k) = \frac{A}{N} \qquad k \neq 0 . \tag{27}$$

Recalling the definition of H(k) in Equation (20), we have

$$R(k) = \frac{A}{N[1-e^{-j2\pi k/N}]} \qquad k \neq 0 . \tag{28}$$

Therefore, we observe that when dealing with a step-like waveform such as f(t) in Figure 18, the truncation problem can be avoided and N - 1 samples of the true Fourier Transform (DC excluded) obtained if we first form the DFT of f(t) and then add to it R(k). Mathematically, we start with f(t) and form the ordinary DFT coefficients F(k) according to Equation (13). Next, we form

$$F'(k) = F(k) + \frac{A}{N[1-e^{-j2\pi k/N}]} \qquad k \neq 0 \quad (29)$$

which we regard as a modified DFT.

As an example of the application of the ordinary DFT, Equation (13), and modified DFT, Equation (29), to a step-like waveform, consider the delayed unit step function shown in Figure 22:

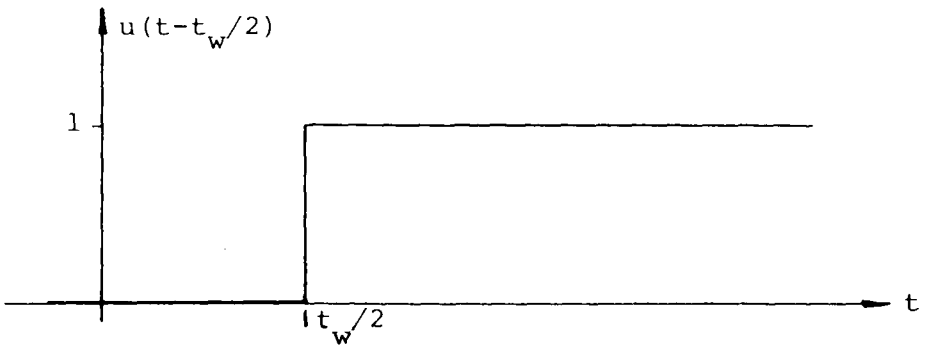

Figure 22 A waveform used to illustrate both the necessity and the utility of the modified DFT.

The true Fourier transform of $u(t-t_w/2)$ is obtained from Equation (14) as

$$U(\omega) = e^{-j\omega\frac{t_w}{2}} \left[\pi\delta(\omega) + \frac{1}{j\omega}\right] . \qquad (30)$$

Next, we form a 32 point ordinary DFT and a 32 point modified DFT of $u(t-t_w/2)$. We will compare the magnitude spectrum of Equation (30) to the magnitude spectrums of the modified DFT and ordinary DFT at the frequencies $k2\pi/t_w \equiv k\omega_o$ $(k\neq 0)$. Results of this are shown in Figure 23, with the solid curve representing $|U(\omega)|$, solid dots representing the magnitude of the modified DFT coefficients $|F'(k)|$, and circles representing the magnitude of ordinary DFT coefficients $|F(k)|$.

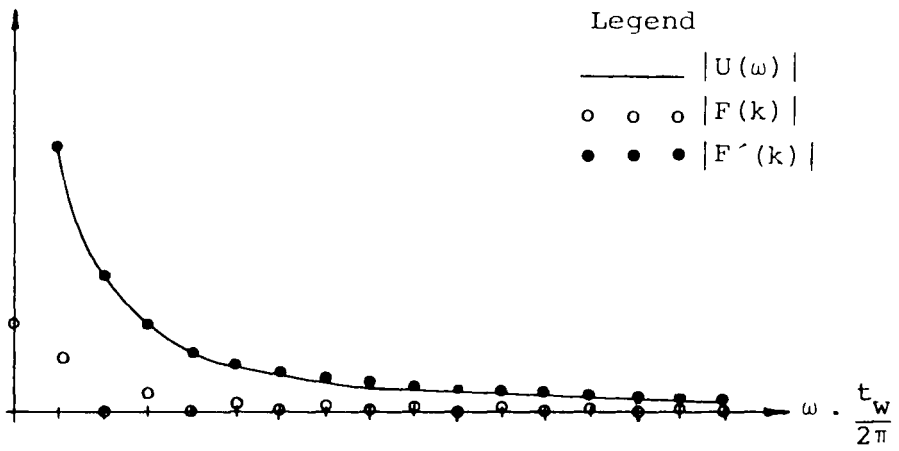

Figure 23 The true Fourier Transform is compared to the ordinary DFT and modified DFT.

As our previous arguments indicated, the ordinary DFT assumes periodicity and computes the Fourier coefficients of a 50 percent duty cycle square wave of period t_w. Hence, the error is great between the circles and solid curve of Figure 23. The excellent agreement between the solid dots and true transform curve of Figure 23 constitutes verification of the validity of the modified DFT, Equation (29). The small errors between the solid dots and the true transform curve evident at higher frequencies are not from approximate validity of the modified DFT, but are due to the fact that the signal $u(t-t_w/2)$ is not bandlimited. Because of this, the 32 samples of $u(t-t_w/2)$ taken to form the DFT do not satisfy the Nyquist condition $\omega_s \geq 2w$ [10]. In fact, it is only possible to approximately reach the Nyquist rate by taking larger numbers of samples (which increases the sampling frequency ω_s) so that the spectrum of the sampled signal is approximately zero at ω_s. This problem is nothing new; every application of digital signal processing must deal with unrealizable ideal situations by approximations.

4.3 Computer Simulation Including Application of Wiener Filtering

At this point we have developed the tools necessary to implement a computer based simulation. In initially implementing this simulation, we will use measured data (for both crosstalk and voltage reflections) at a risetime of 130 picoseconds to generate the TDR transfer function. We will use the slower steps, as obtained through the installation of Hewlett Packard risetime converters, and generate simulation predictions of the responses that should correspond to those slower steps. Then we compare the simulation predictions to measured responses with risetime converters installed.

A notation is now introduced. The steps, which are recorded on an XY plotter and then sampled with a sample interval T_s, are denoted as $s_{n.nnn}(nT_s)$ where n.nnn is the 10 percent to 90 percent risetime in nanoseconds. Correspondingly the responses (voltage reflections or crosstalk) are denoted as $r_{n.nnn}(nT_s)$. When the above signals are transformed by the modified DFT, they are denoted by capital letters as $S_{n.nnn}(k)$ and $R_{n.nnn}(k)$. Finally, the transfer function values at $k\omega_o$ are denoted $H(k)$.

With the previous notation developed, a flowchart of the overall computer simulation process is presented in Figure 24.

The system is illustrated predicting the response $r_{2.00}(nT_s)$, and the following discussion is phrased accordingly. However, the discussion applies in general. The rectangular boxes represent Fortran computer programs. The corresponding names are indicated inside the boxes. The parenthesized quantities indicate what mode a particular program is operating in, as explained below.

Program .SFFTB implements the standard Discrete Fourier Transform by the use of the Cooley-Tukey algorithm [4]. This forward Discrete Fourier Transform is indicated by the parenthesized "F". Immediately following program .SFFTB is program .SMODB, which implements the modification to the Discrete Fourier Transform. It operates in the forward mode. Programs .SFFTB and .SMODB are always used in conjunction, and the modes of operation correspond. Their combined operation in the forward mode generates samples in frequency of the true Fourier Transform. Alternatively, both these programs can operate in the inverse mode, indicated by parenthesized "I", and

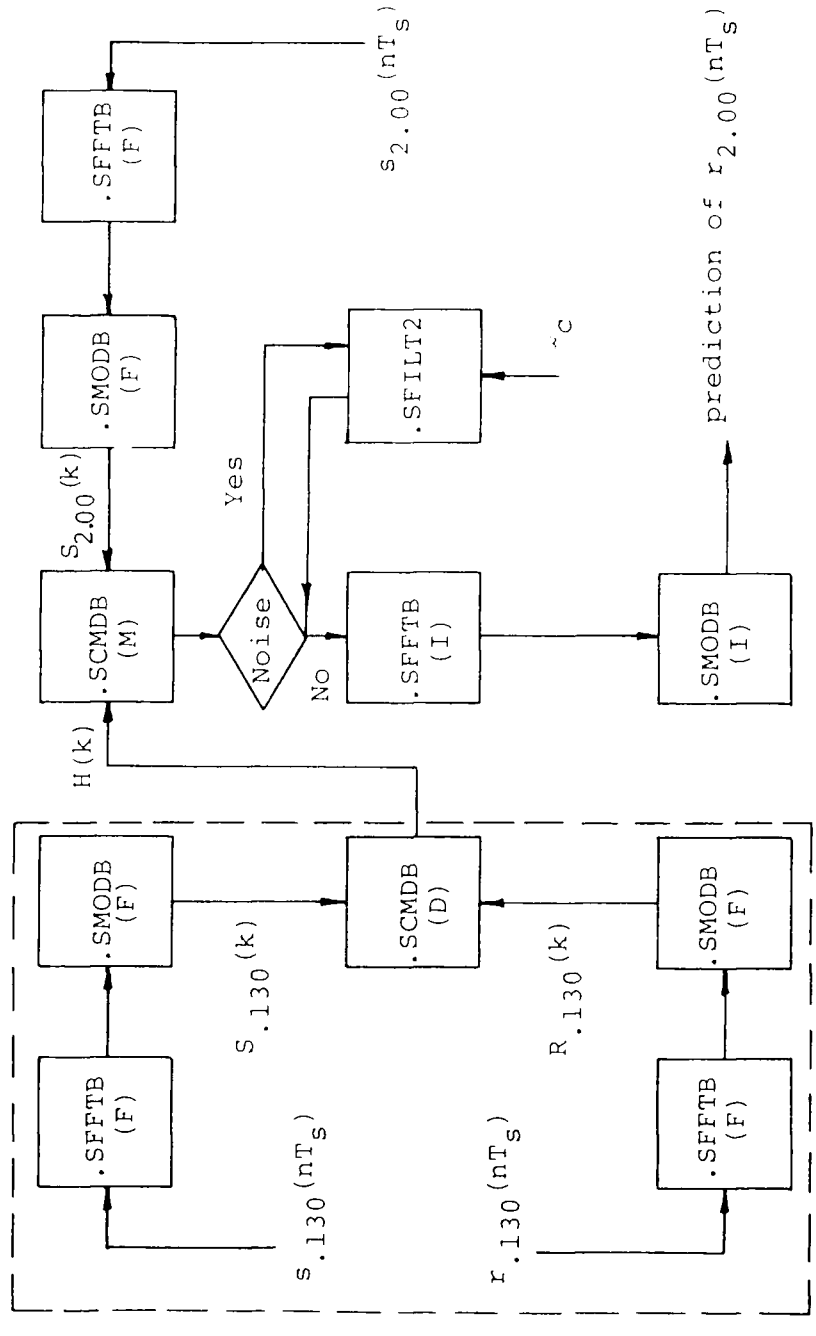

Figure 24 A flowchart of the computer based simulation process.

their combined operation serves as an inverse Fourier Transform that generates samples in time of the signal.

Program .SCMDB provides multiplication (Mode "M") or division (Mode "D") of complex quantities. The two inputs to this program will be complex sequences of length N, where N is the number of samples taken to represent the various time functions. Corresponding elements of these sequences are multiplied or divided to form the corresponding element in the output sequence.

The flow of operations in the computer based simulation process is now discussed. First, the sampled fast step $s_{.130}(nT_s)$ and the corresponding sampled response $r_{.130}(nT_s)$ are both Fourier transformed and their transforms divided in order to obtain the transfer function H(k). This operation is indicated within the dashed line box, and is performed only once. Next, samples of the step $s_{2.00}(nT_s)$ are Fourier transformed to yield $S_{2.00}(k)$. Then in accordance with standard linear system analysis, the transfer function H(k) is multiplied by $S_{2.00}(k)$, and the result is the Fourier Transform of the simulation prediction. This is now inverse Fourier transformed, and the samples of the prediction are obtained.

When this prediction is obtained, it is possible that it will contain noticeable noise. Several factors contribute to this noise. First, the TDR system will exhibit shot noise from the resistors utilized in the circuitry. This can be broad band noise. Secondly, environmental noise from nearby wiring can contribute to system noise. Thirdly, the TDR equipment characteristically suffers from jitter of the display. This effect has the appearance of being caused by a loose connection, but attempts to locate it prove futile. A better explanation of display jitter relies on the realization that the sampling oscilloscope processes thousands of waveforms in order to display one trace. If any one of these waveforms is corrupted, the entire trace will display jitter.

Another important origin of noise are errors made in sampling the signals from the recorded XY plots. This simply means that if the signal value at time nT_s is $f(nT_s)$, the sample value is erroneously taken to be $f(nT_s) + \delta$. The error δ results from graphical interpolation which is not exact. If this type of error occurs at each sample point, it is quite reasonable to expect the values of δ to be Gaussian distributed. In addition, we expect them to be uncorrelated. This type

of noise process is white noise [20].

In order to deal with the noise problem, it was felt that a general method of optimal filtering should be incorporated into the simulation process. This would allow its use at any future time when noise became a problem. Given that we have the desired signal s(t) obscured by uncorrelated noise n(t), we introduce a linear filter $H_w(\omega)$ as indicated in Figure 25:

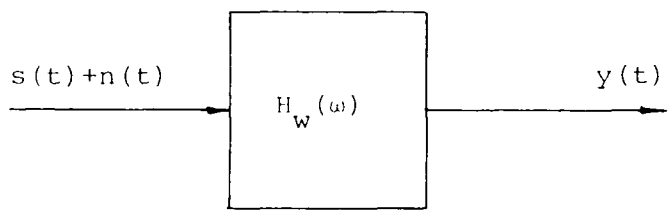

Figure 25 The Wiener filter $H_w(\omega)$ is introduced.

Wiener's theory [9] prescribes that the mean square error between y(t) and s(t) be a minimum. The functional form of $H_w(\omega)$ can then be determined in terms of the power density spectrums of s(t) and n(t). Denoting the power density spectrums of s(t) by $S_s(\omega)$

and of n(t) by $S_n(\omega)$, it can be shown that [9]

$$H_w(\omega) = \frac{S_s(\omega)}{S_s(\omega) + S_n(\omega)} \quad . \tag{31}$$

Now we must introduce suitable approximations in order to apply Equation (31) to the TDR prediction problem. We shall follow the usual assumption that the noise is white. This properly describes noise resulting from sampling errors as well as noise in the system as a whole. In addition, the assumption of white noise provides some mathematical simplicity. White noise has a power density spectrum given by

$$S_n(\omega) = \frac{n}{2} \quad . \tag{32}$$

In order to determine $S_s(\omega)$, it was assumed that $S_s(\omega) = K/\omega^N$, and the unknown constant N determined by a least squares analysis with the power density spectrums of representative signals from this project. This analysis indicated we should assume

$$S_s(\omega) = \frac{K}{\omega^2} \tag{33}$$

which yields

$$H_w(\omega) = \frac{1}{1 + (\frac{\omega}{\omega_c})^2} \quad , \tag{34}$$

where the cutoff frequency is given by

$$\omega_c = \sqrt{\frac{2K}{n}} \quad . \tag{35}$$

Equation (35) is reasonable in that as the signal to noise ratio K/n increases, the cutoff frequency ω_c moves further out.

The filter has been designed as an analog filter, and if it were implemented in a truly analog situation the Fourier Transform of the noisy signal would be multiplied by the filter transfer function. Since we have N samples of the Fourier Transform of the noisy signal, we will implement the multiplication at these points. The N samples of the filter are given by

$$H_w(k) = \frac{1}{1 + \left(\frac{k\omega_o}{\omega_c}\right)^2} \qquad k = 0,1,2,\ldots,N-1 \tag{36}$$

where $\omega_o = 2\pi/t_w$. The filter is realized in program .SFILT2, and the process flowchart of Figure 24 indicates how it is applied.

The determination of the appropriate cut-off frequency ω_c is now illustrated. The magnitude spectrum of a typical noisy signal is depicted in Figure 26:

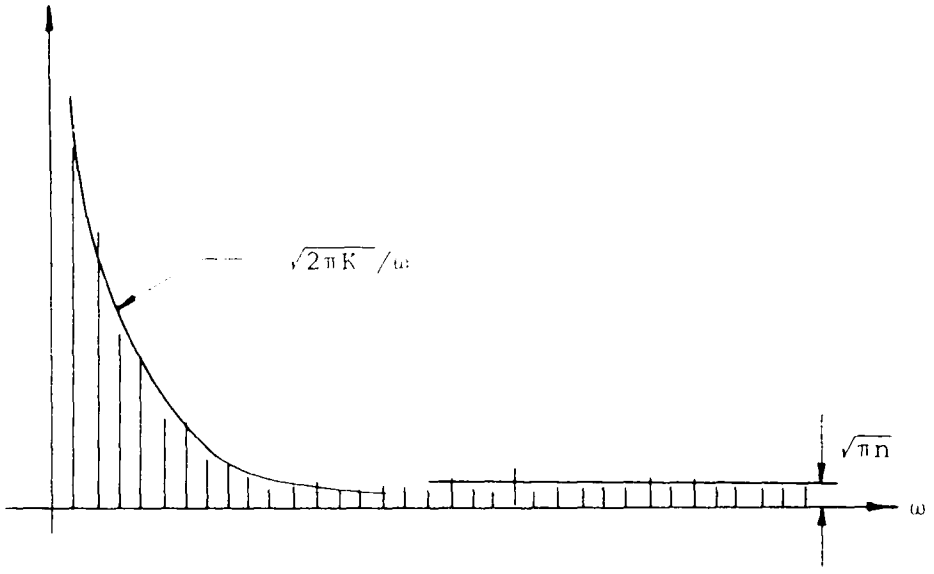

Figure 26 Relating to the estimation of the signal to noise ratio.

As illustrated, the value of K is determined from fitting the lower frequency coefficients of the magnitude spectrum to a curve of the form $\sqrt{2\pi K}/\omega$, which follows from Equation (33) through the relationship between the magnitude spectrum and power density spectrum [9]. Likewise, n is determined by equating the apparent noise level to $\sqrt{\pi n}$.

The critical reader may recall the modification to the DFT will be incorrect for the DC term (k=0).

Mathematically, this difficulty arises because the true Fourier Transforms of $s_{.130}(t)$ and $r_{.130}(t)$ contain impulses at $\omega = 0$. This problem is avoided by realizing that both $s_{.130}(t)$ and $r_{.130}(t)$ are step like waveforms that are zero for negative times and each reach constant values $s_{.130}(t_w)$ and $r_{.130}(t_w)$ at time t_w, as indicated in Figure 27:

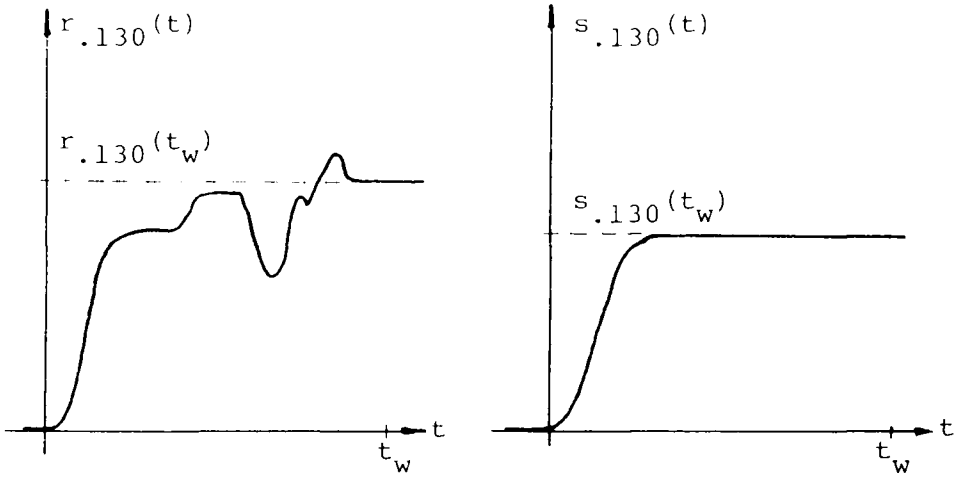

Figure 27 Typical reflection plot and voltage step plot.

Since $[o,t_w]$ is a finite domain, and the signals are assumed to exist at a constant level for all times beyond t_w, the ratio of the DC content of $r_{.130}(t)$ to the DC content of $s_{.130}(t)$ will be given by [10]:

$$\frac{\pi\delta(\omega)r_{.130}(t_w)}{\pi\delta(\omega)s_{.130}(t_w)} = \frac{r_{.130}(t_w)}{s_{.130}(t_w)} . \qquad (37)$$

Therefore, we predict the DC content of $r_{2.00}(t)$ to be

$$\pi \left[\frac{s_{2.00}(t_w)\ r_{.130}(t_w)}{s_{.130}(t_w)}\right] \delta(\omega), \qquad (38)$$

which determines the signal level $r_{2.00}(t_w)$ to be the bracketed factor in Equation (38). In addition to this new information, we also know all signals are causal, so $r_{2.00}(t)$ should be zero for negative times. Given these two facts, the inverse mode of program .SMODB is able to correctly extract a predicted waveform.

5. Experimental Verification

At this point we have developed the simulation process. First we will deal with voltage reflection predictions. A specimen is selected for testing, typically several feet of microstrip line with several discontinuities. The driven end is fed from a solder connection to RG187/U coaxial line. RG187/U

was selected because its characteristic impedance is 75 ohms, which is close to typical microstrip impedance levels. Of course, as far as voltage reflections are concerned, any mismatch between coaxial line and microstrip will be considered part of the system under test. Another factor in the selection of RG187/U is its small size and flexibility. The solder connection between the coaxial line and the microstrip becomes part of the system under test, and must not be changed during testing. The RG187/U coaxial line is fed from the directional coupler by a 50 ohm airline. This airline provides an impedance reference level on the voltage reflection plots.

Data are recorded on an XY plotter with the TDR unit in the record mode. This mode produces a sweep time of nearly 60 seconds, during which time the signal being plotted is averaged.

Data were collected for the voltage reflection or impedance plot of a sample when excited by the unslowed step output of the HP 1415 TDR unit. This step has a 10 percent to 90 percent risetime of 130 picoseconds. Also, a 50 ohm load was installed in place of the sample and the TDR impedance plot recorded. This latter case will show no reflections, since the

step generator output impedance is also 50 ohms. Consequently, the TDR impedance plot will be a plot of the generated voltage step. These two plots are used to generate the TDR transfer function. Next, one of the risetime converters is installed and XY plots of the slower step and corresponding response are obtained. The plot of the slower step is then used in conjunction with the TDR transfer function to predict the response. This prediction is then compared with the measured response plot. This prediction and comparison is generally done for the .5 nanosecond, 1 nanosecond, and 2 nanosecond risetime converters.

We will now show the results of TDR voltage reflection predictions. The particular sample considered was a microstrip line, the dimensions of which are given in Figure 28:

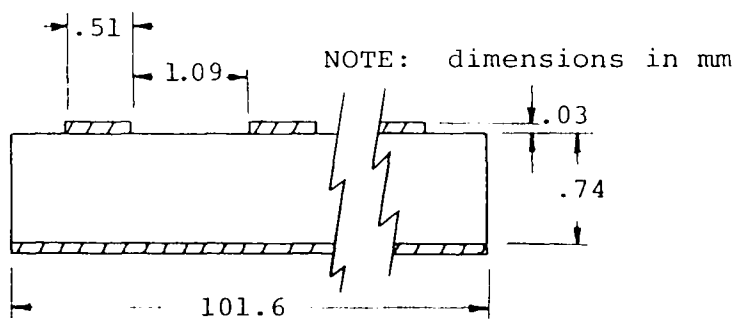

Figure 28 The dimension specifications of the TDR sample.

The microstrip was fed from a solder connection to RG187/ U. In addition to the inevitable discontinuity at the soldered joint, additional discontinuities were placed along the microstrip, as Figure 29 depicts from a top view:

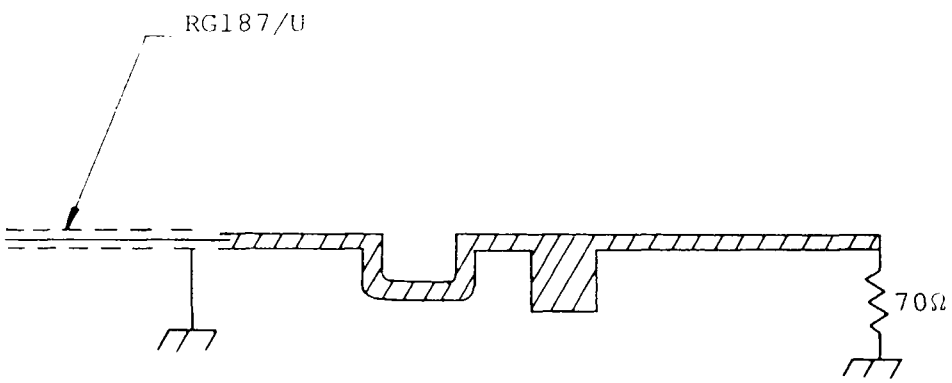

Figure 29 The details of the microstrip conductor discontinuities.

The enlarged conductor area, or capacitive pad, might represent a midline high input impedance tap. Some microstrip lines include these small capacitive pads for logic probe test points. The lateral conductor diversion might represent the signal conductor having to avoid another conductor. It is noted that while faster switching speeds and smaller devices encourage greater system packaging density, increasing system

density results in more conductor diversions being required. At the same time, the aforementioned faster switching speeds cause conductor diversions to create serious voltage reflections.

The measured voltage reflection response from a 130 picosecond step is shown in Figure 30. Figure 30 shows the voltage step, then the 50 ohm airline, then 70 ohm coaxial line, and finally the microstrip line. In this case the impedance of the microstrip is slightly greater than the coaxial line. The relatively smooth transition (or lack of large reflection) from coax to microstrip indicates an unusually good solder joint. Greater detail would be available from expansion of the vertical scale, but clearly the solder joint is not the most significant discontinuity along the line. The capacitive pad and conductor diversion have produced a large reflection. Unlike the resistive reflections (for example the reflection due to the change from 50 ohm airline to 70 ohm coax) which are frequency independent, the capacitive pad and conductor diversion create a reactive discontinuity that is frequency dependent.

From 128 samples of the 130 picosecond step and corresponding voltage reflection response, the TDR process sequence generates the TDR transfer function

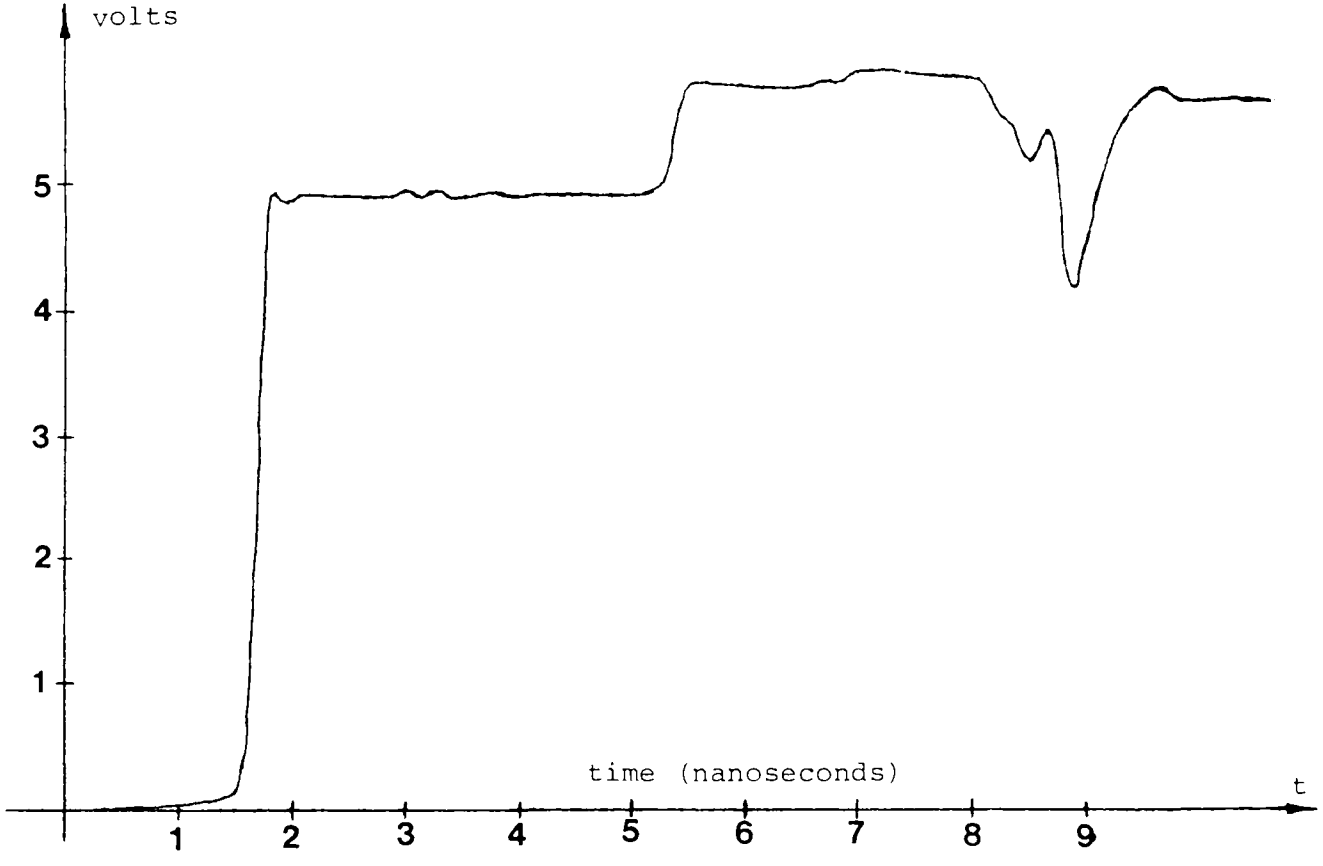

Figure 30 Measured voltage reflections with a 130 picosecond risetime.

H(k). If the transmission system were a uniform 50 ohm system there would be no reflected waves and the TDR response would just be the input step. This ideal situation would yield a TDR transfer function that was unity for all frequencies. The TDR transfer function corresponding to the nonideal microstrip system under consideration is found to deviate from unity at most frequencies.

The transfer function represents an intermediate mathematical step in the context of this project; however, great interest has been expressed by design engineers wishing to extract design information from this voltage reflection transfer function and the forthcoming crosstalk transfer function.

With the transfer function stored in computer memory, the TDR process sequence was used in conjunction with 128 samples of the slower steps to make predictions of the slower responses. These predictions are then compared to measured responses. These comparisons are presented in Figures 31A-C, where the solid curve is the measured data and the dots are the 128 sample points of the predicted waveform. The predictions are shown for the .5 nanosecond step, 1 nanosecond step, and 2 nanosecond step. Wiener filtering

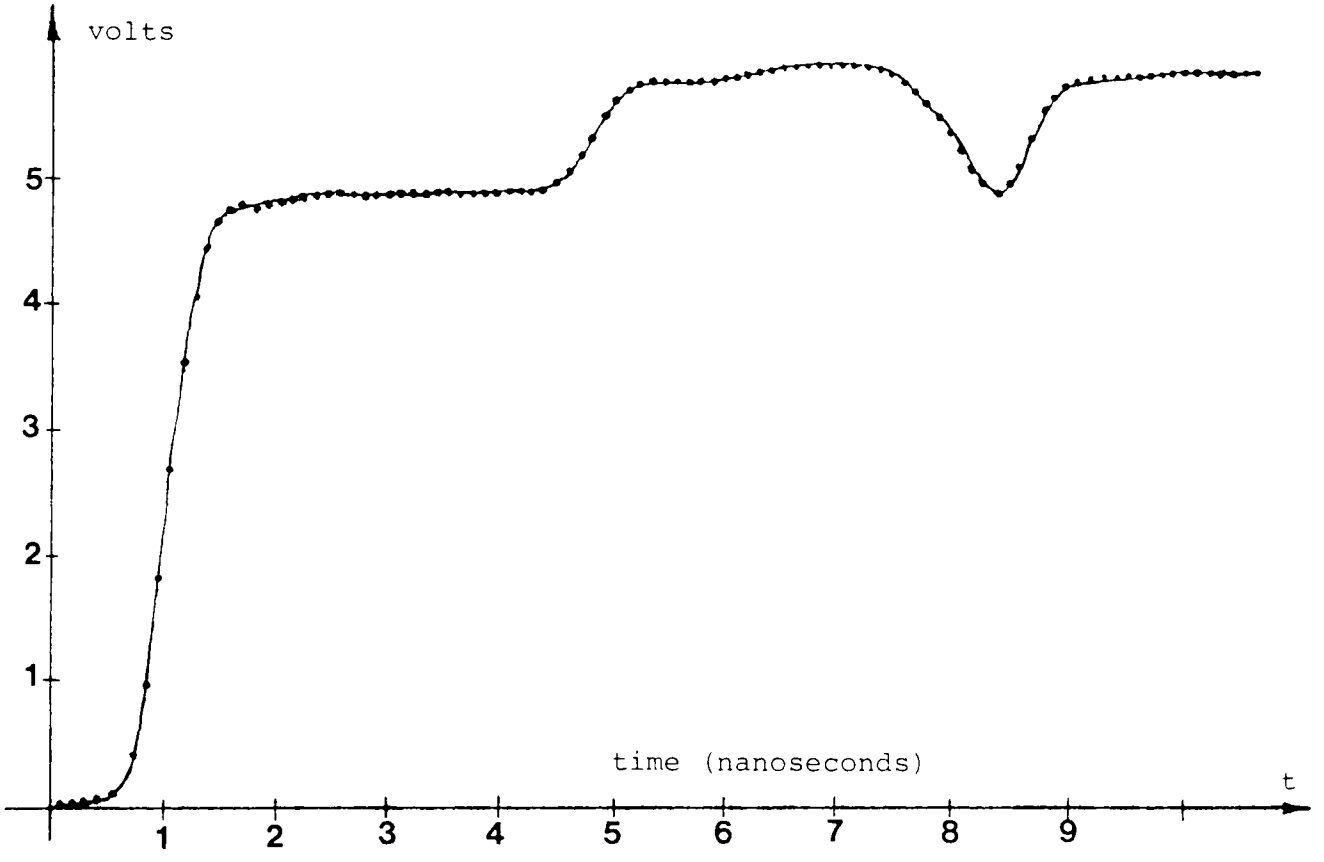

Figure 31A Comparison of simulation prediction (dots) to measured voltage reflections with a .5 nanosecond risetime.

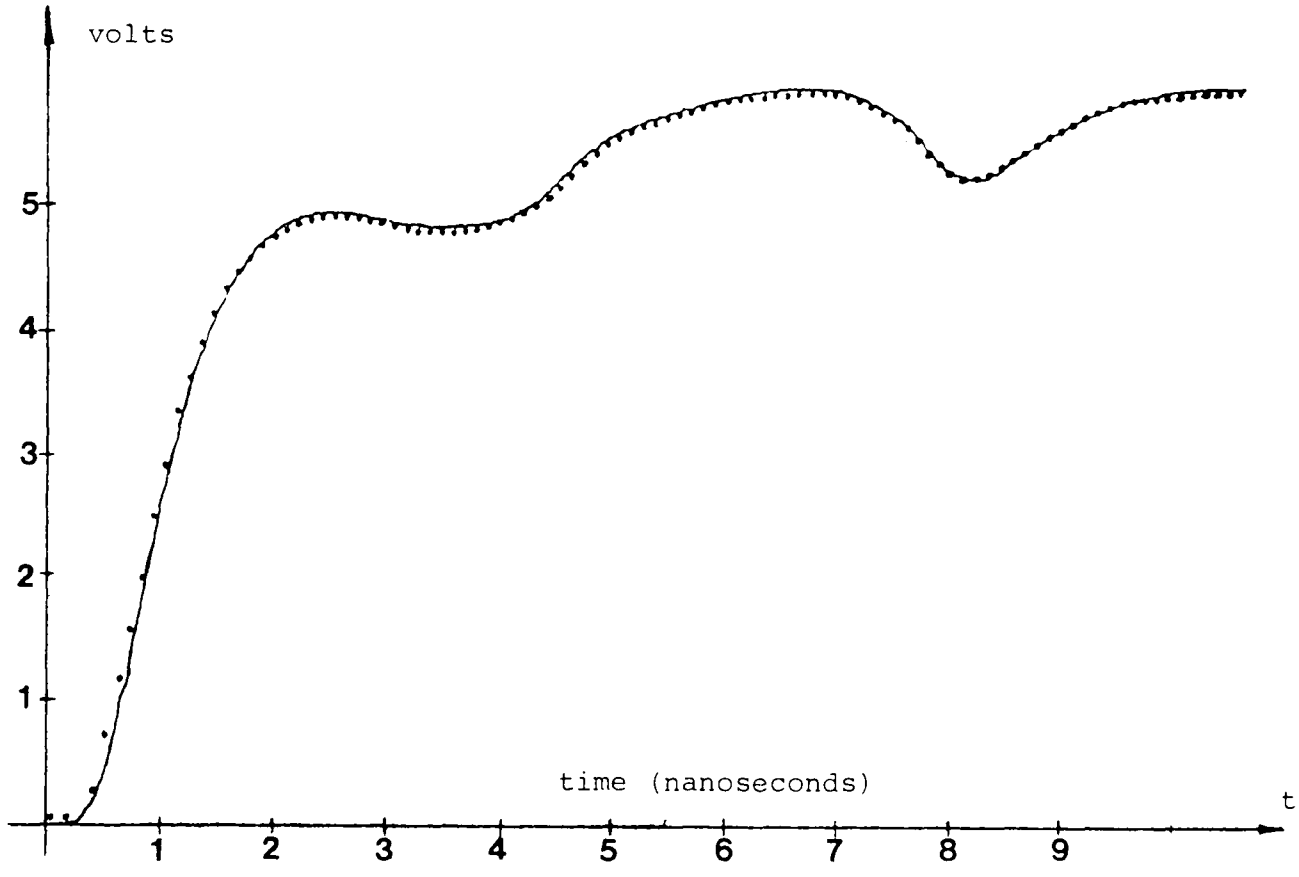

Figure 31B Comparison of simulation prediction (dots) to measured voltage reflections with a 1 nanosecond risetime.

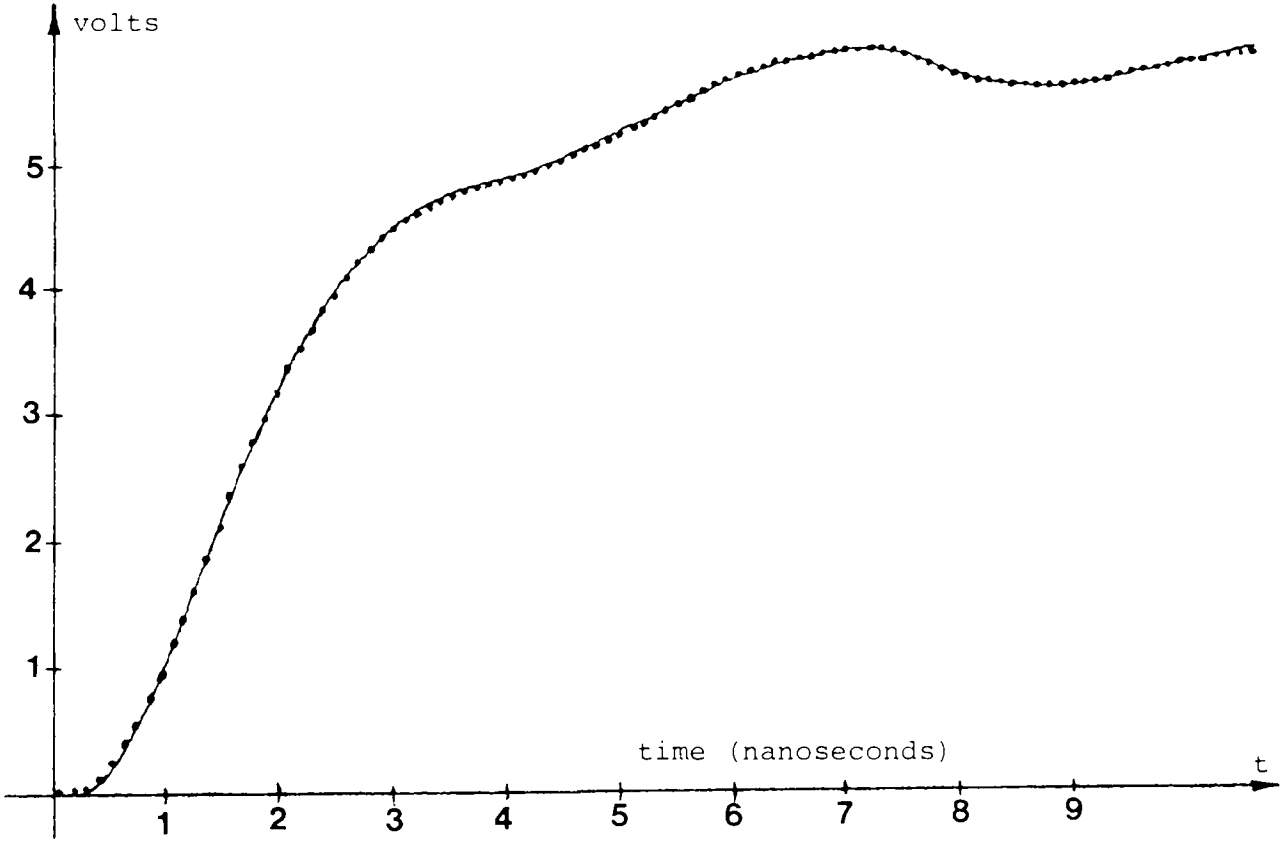

Figure 31C Comparison of simulation prediction (dots) to measured voltage reflections with a 2 nanosecond risetime.

is not required in these predictions. The agreement between solid curve (measured data) and dots (simulation predictions) is seen to be excellent. We will briefly present the results of another TDR prediction. The sample used for this second prediction was a microstrip line with 13 signal conductors and solid ground plane. Each conductor has a .9cm long cylindrical vertical pin soldered onto it, as indicated in Figure 32:

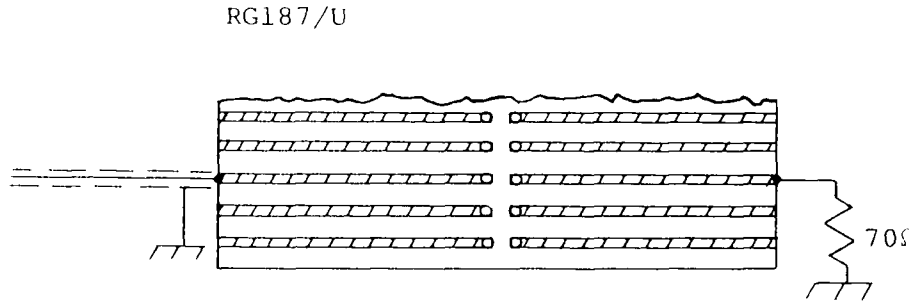

Figure 32 The microstrip sample used in the second TDR simulation.

These pins allow a push-on connector to attach a 25 meter flat ribbon cable to the line. The TDR signal was launched into line 9 by a solder junction to RG187/U coax. The far end of line 9, both ends of

the remaining 12 lines, and the far end of the flat ribbon cable were terminated in their characteristic impedance, which is near 70 ohms.

The measured reflections resulting from the 130 picosecond step are presented in Figure 33.

The characteristic impedance of the coax and microstrip are near 70Ω. The largest reflection is coming from the connector. Comparison of the general shape of the reflection with Figure 11 indicates an inductive effect. This occurs because the effective signal path and ground path become further separated when passing through the connector.

The comparison between measured data and the predictions of the simulation process are given in Figures 34A-C. Again, Wiener filtering is not required. The agreement is excellent.

The simulation procedure is also applicable to crosstalk. A 30cm section of 3 conductor microstrip was tested for crosstalk levels, and the results of testing with a 130 picosecond step are given in Figure 35.

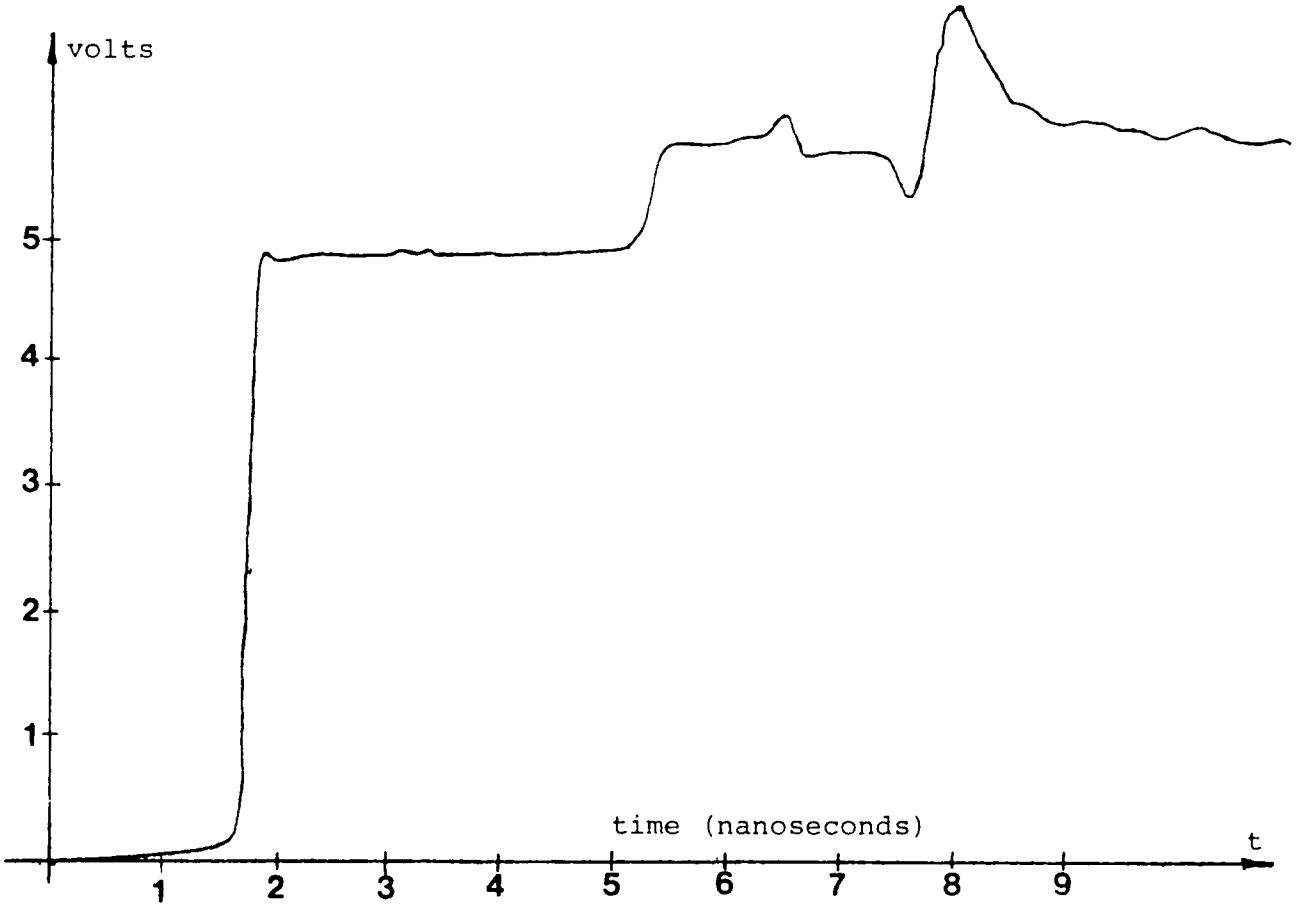

Figure 33 Measured voltage reflections with a 130 picosecond risetime.

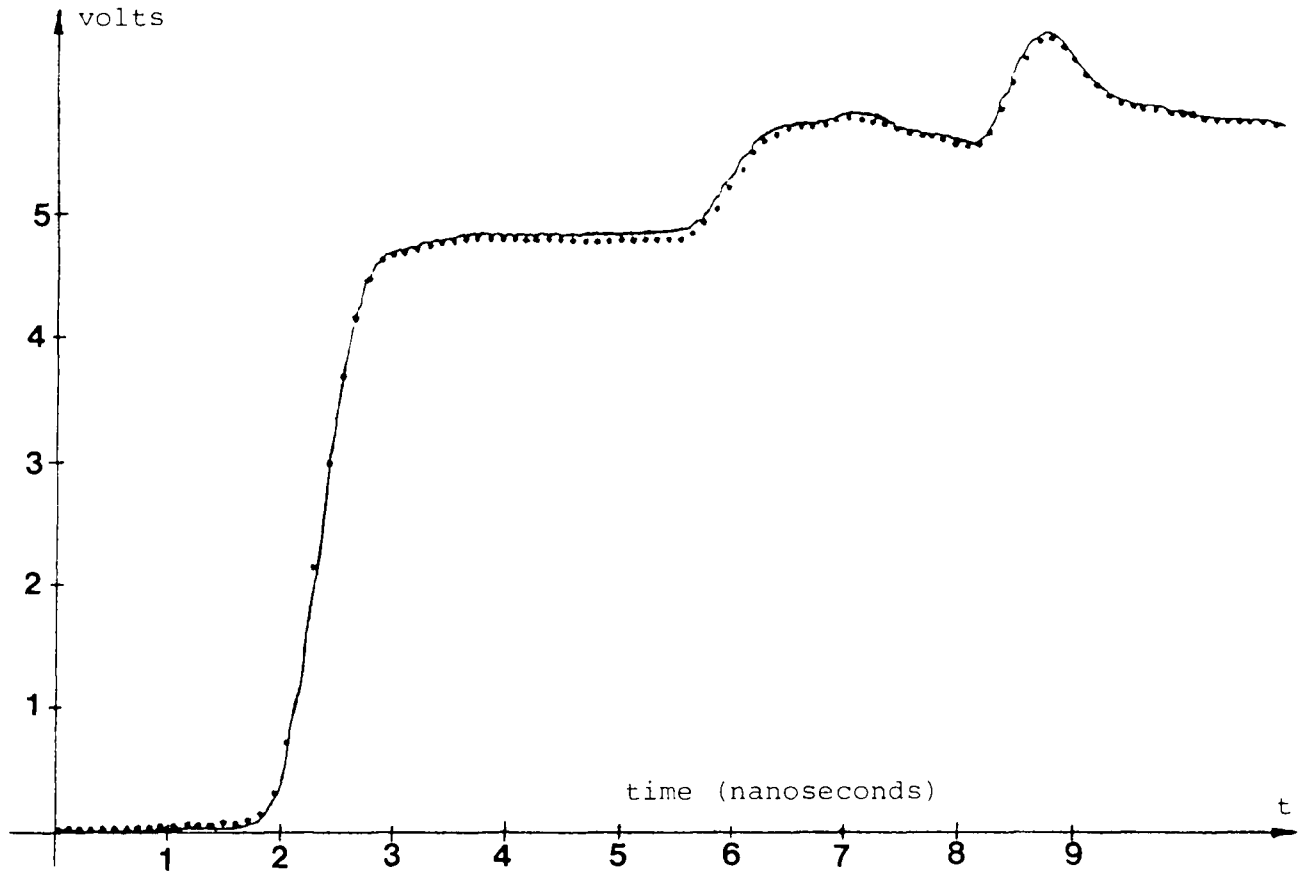

Figure 34A Comparison of simulation prediction (dots) to measured voltage reflections with a .5 nanosecond risetime.

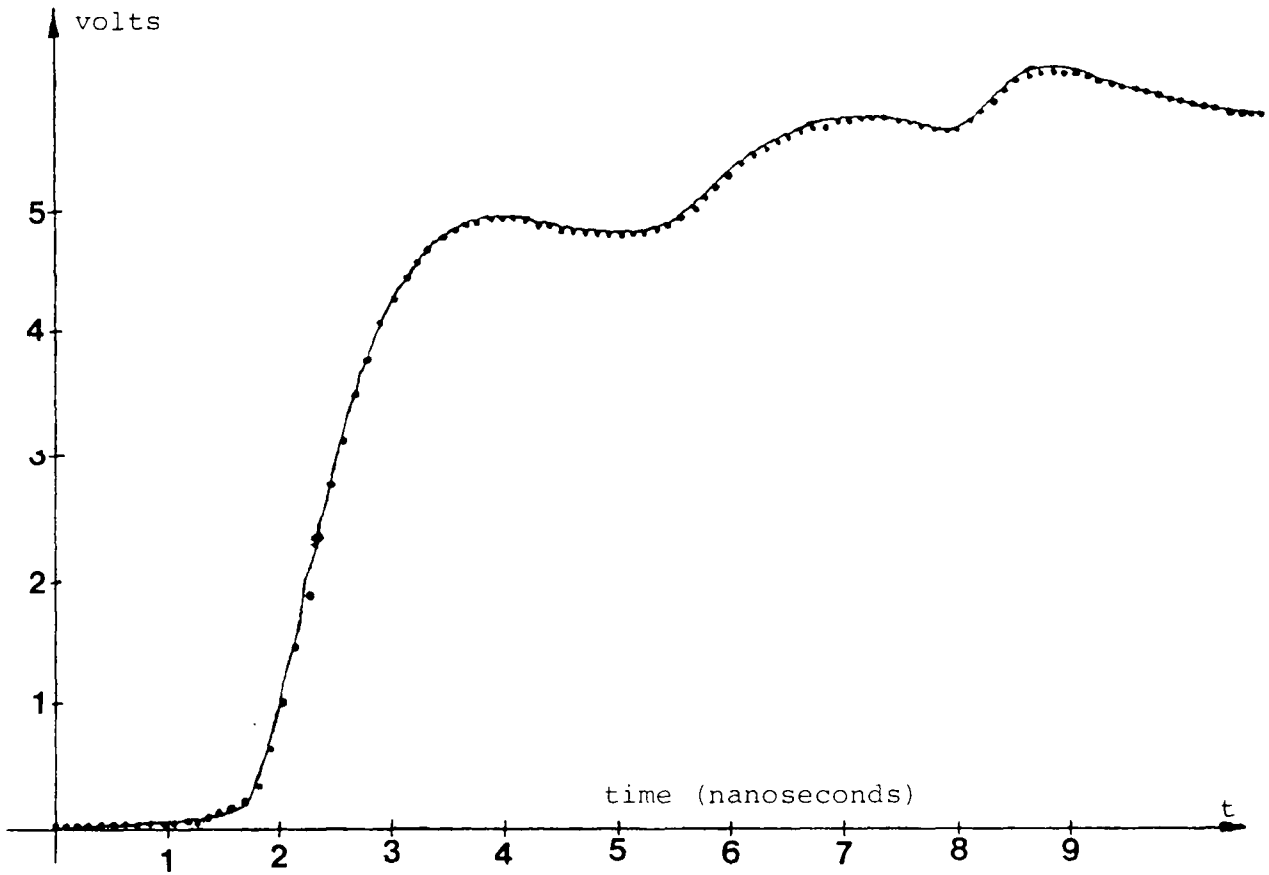

Figure 34B Comparison of simulation prediction (dots) to measured voltage reflections with a 1 nanosecond risetime.

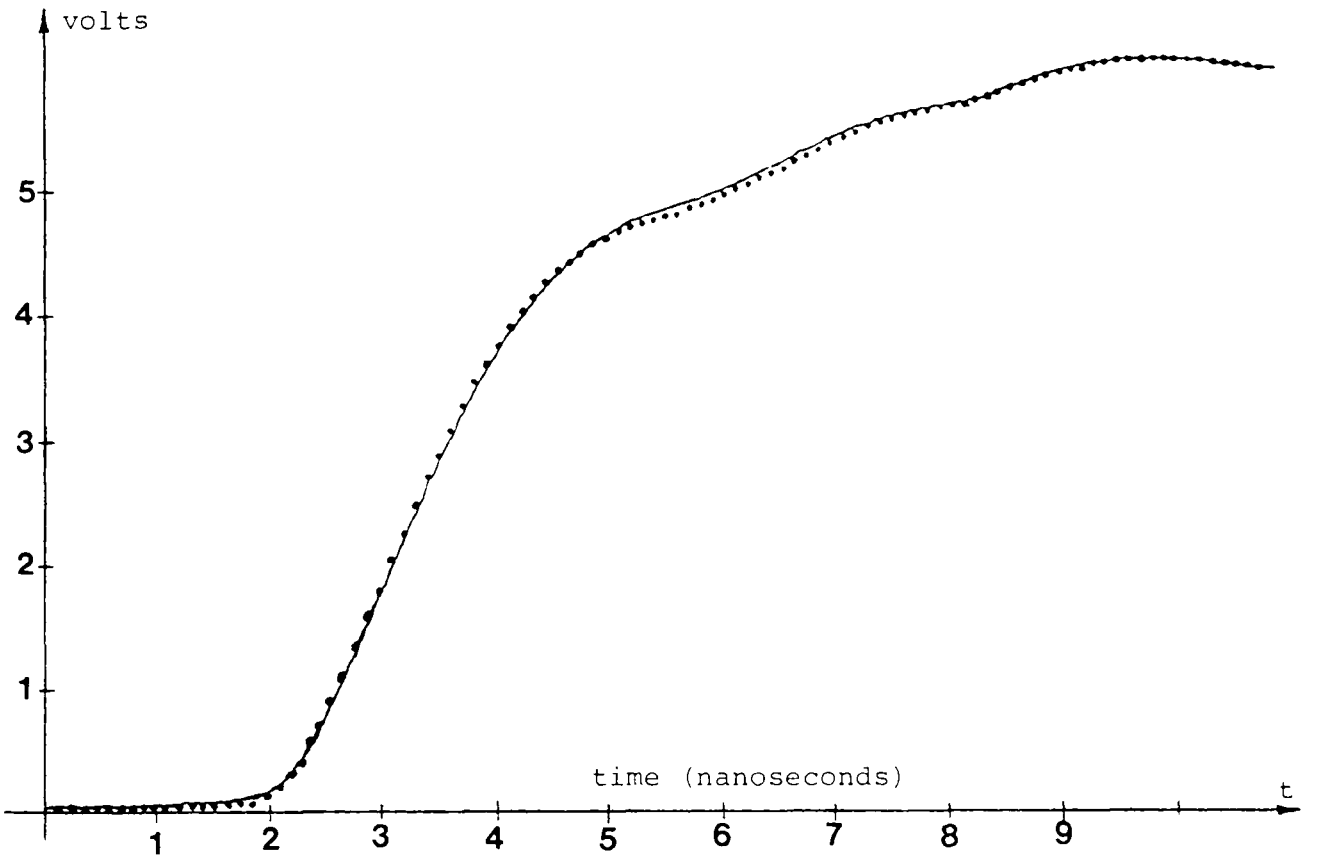

Figure 34C Comparison of simulation prediction (dots) to measured voltage reflections with a 2 nanosecond risetime.

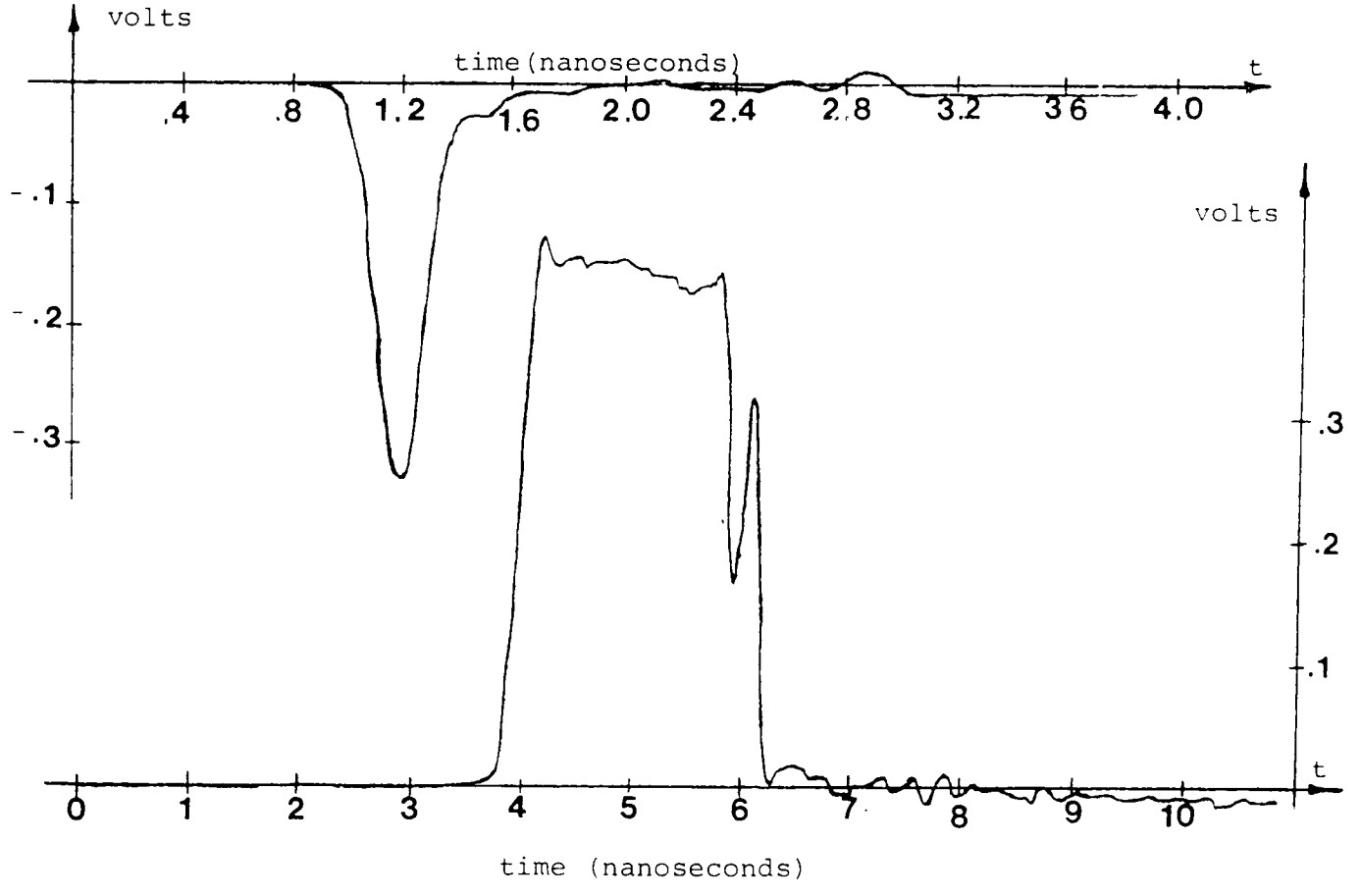

Figure 35 Measured forward crosstalk (upper axes) and measured back crosstalk (lower axes) with a 130 picosecond risetime.

The results are reasonable when comparison to Figures 7 and 8 is made. The oscillatory behavior evident in the backward crosstalk pulse is actually forward crosstalk reflected from an imperfect termination at the far end of the quiet line. Its existence will be a good test for the TDR prediction process. The same process as used for reflection predictions was used for crosstalk predictions. The need to modify the DFT for step like waveforms does not in general exist in crosstalk predictions because the signals start and end at level zero. This causes program .SMODB to implement Equation (29) by adding zeroes (since A = 0 in Equation (29)), and .SMODB is effectively inoperative. Predictions were made for forward and backward crosstalk at .5, 1 and 2 nanoseconds. All the predictions exhibited some noise. A representative example of this is the predicted 1 nanosecond forward crosstalk, shown in Figure 36:

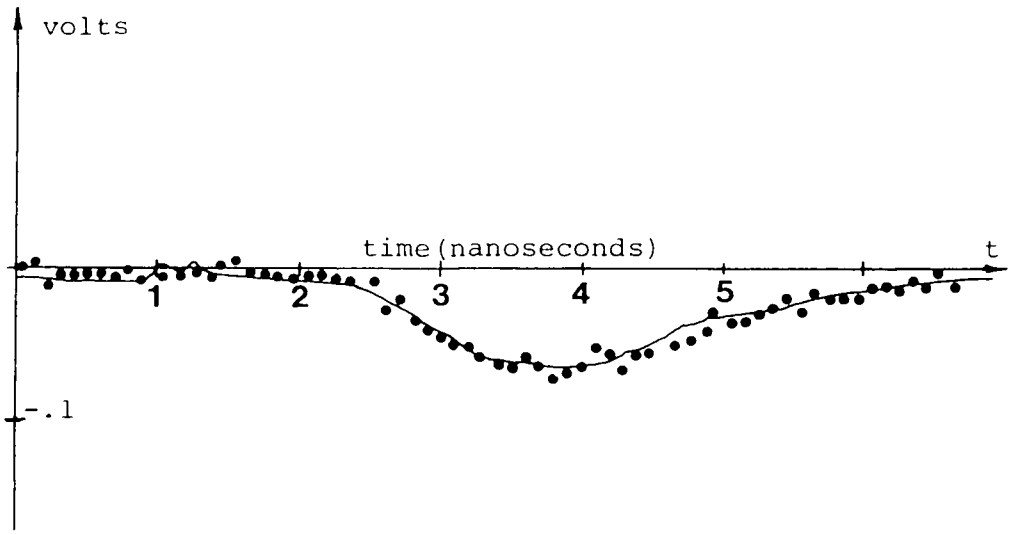

Figure 36 The measured and predicted 1 nanosecond forward crosstalk.

The noise is due to the fact that the crosstalk signals, especially the forward crosstalk signals, are much higher frequency signals than the previously dealt with voltage reflection signals. One method of realizing this is to examine the crosstalk transfer function H(k) which is an intermediate result of the crosstalk prediction process. This transfer function is given in Figure 37, and is seen to be roughly high-pass. This is expected since the coupling is largely capacitive.

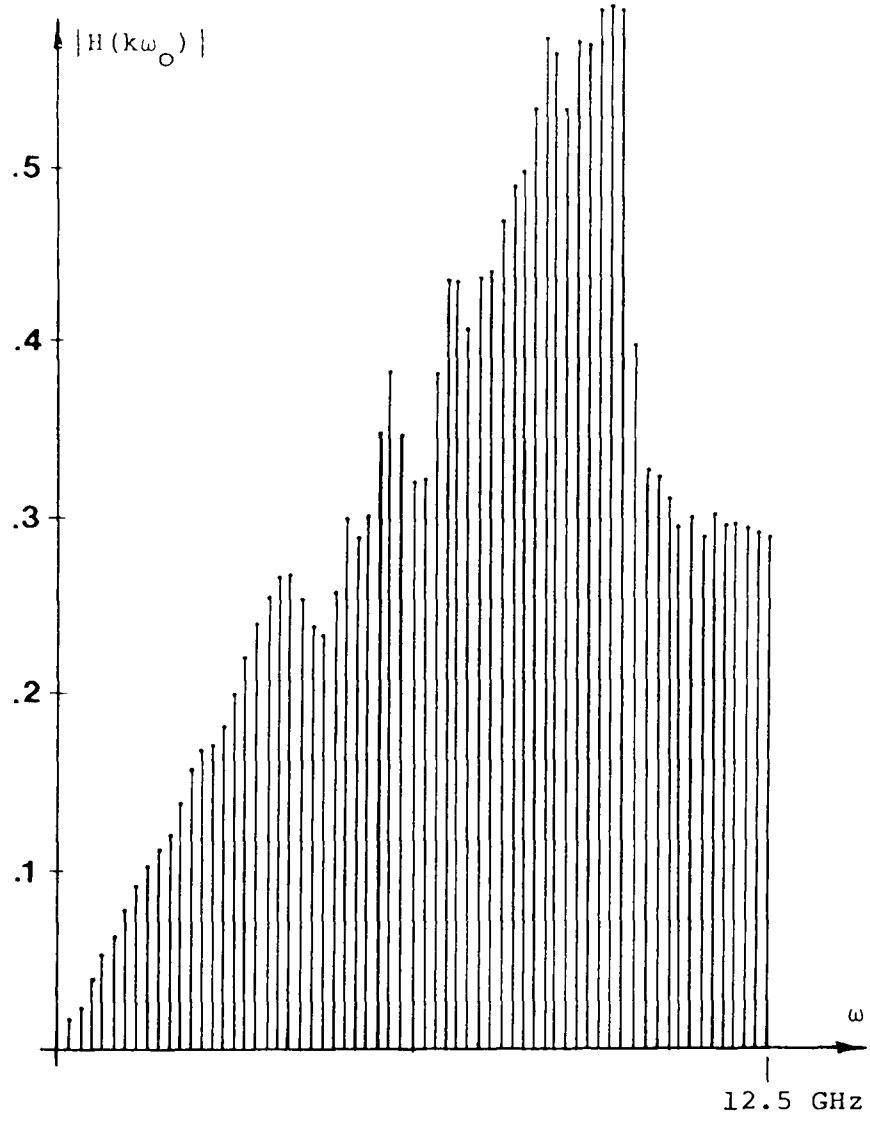

Figure 37 The transfer function for forward crosstalk.

As pointed out earlier, the transfer function is an intermediate result, but tremendous interest has been expressed in particularly the crosstalk transfer

function being a design aid. The crosstalk transfer function gives the ratio of the frequency content of the quiet line crosstalk voltage to frequency content of the excitation voltage.

In view of the noisy prediction shown in Figure 36, we elected to implement the Wiener filtering program .SFILT2. The results of this optimal filtering are shown in Figures 38 A-B. Figure 38A shows the 1 nanosecond forward crosstalk prediction after Wiener filtering. The cutoff frequency ω_c, determined by the method shown Figure 26, is given in Figure 38A. Figure 38A should be compared to Figure 36, and the improvement noted. Additionally we have presented Figure 38B, which shows the prediction of 1 nanosecond back crosstalk. Wiener filtering was also used in this prediction, and the corresponding value of ω_c is given in the figure. Note the simulation process correctly handled the reflected forward crosstalk that was evident in Figure 35.

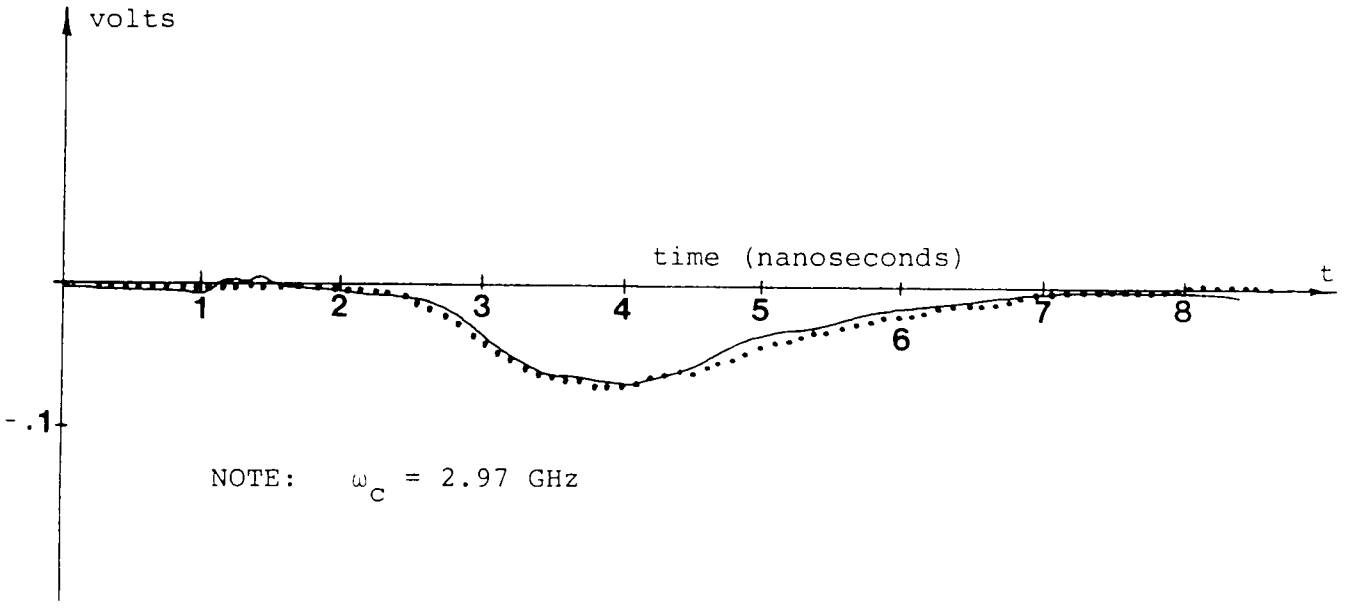

Figure 38A Comparison of Wiener filtered simulation prediction (dots) to measured forward crosstalk with a 1 nanosecond risetime.

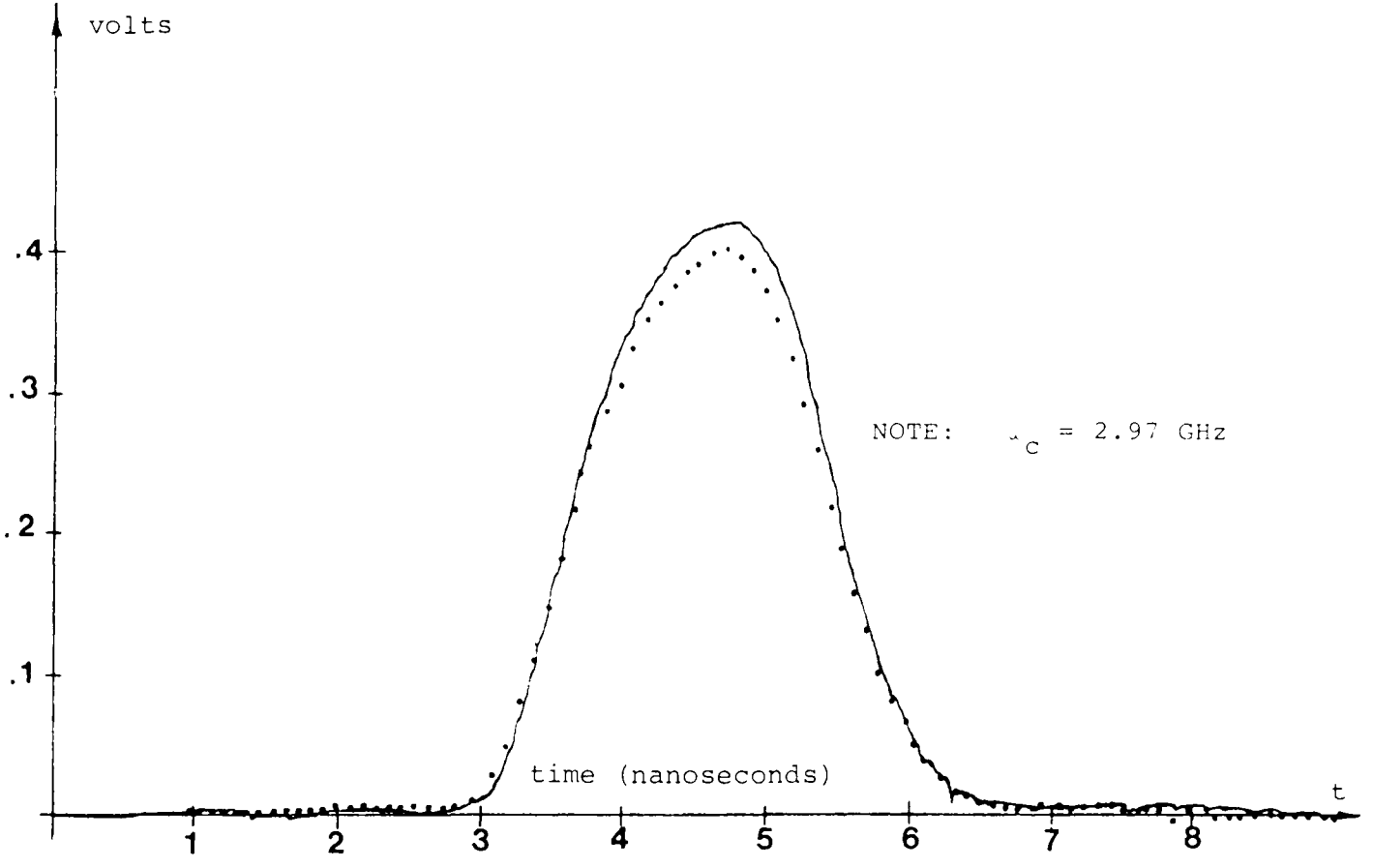

Figure 38B Comparison of Wiener filtered simulation prediction (dots) to measured back crosstalk with a 1 nanosecond risetime.

6. Conclusions

The simulation procedure predictions show good agreement. The small error can easily be shown to be within experimental limitations. Optimal filtering has been successfully used to remove noise. Excellent agreement in both the reflection studies and the crosstalk studies has established complete confidence in the TDR prediction process. It is an extremely powerful tool, since not only the major effects are correctly predicted, but in addition, any higher order effect that is linear is also correctly predicted. For example, we saw that in the measurement of back crosstalk some reflected forward crosstalk appeared. The TDR prediction process handled this complication. In addition, the problem of multiple reflections due to non-ideal 50Ω generator impedance is also correctly handled.

The development and testing of the TDR prediction process is now complete. An example of the process application in industry will now be given. We consider a situation in which a customer expresses the desire to use a particular digital interconnection fixture. He provides the fixture manufacturer with a plot of the waveform in his digital system. The manufacturer has the transfer functions for both

reflection and crosstalk studies stored in computer memory. Equipment exists that can automatically digitize the customer's waveform, and then voltage reflection and crosstalk predictions can be made. The point is that these predictions are tailored specifically to the user's system.

References

[1] Brigham, E. Oran, The Fast Fourier Transform, Englewood Cliffs, New Jersey: Prentice-Hall, Inc., 1974, pp. 91-109 and 132-147.

[2] Catt, Ivor, "Crosstalk (noise) in Digital Systems", IEEE Transactions on Electronic Computers, Vol. EC-16, December 1967, pp. 743-763.

[3] Collin, Robert E., Foundations for Microwave Engineering, New York: McGraw-Hill Book Company, Inc., 1966, pp. 270-273.

[4] Cooley, J.W. and Tukey, J.W., "An Algorithm for the Machine Calculation of Complex Fourier Series", Math. Computation, Vol. 19, 1965, pp. 297-301.

[5] DeFalco, John A., "Reflection and Crosstalk in Logic Circuit Interconnections", IEEE Spectrum, Vol. 7, No. 7, July 1970, pp. 44-49.

[6] Feller, A., Kaupp, H.R. and Digiacomo, J.J., "Crosstalk and Reflections in High Speed Digital Systems", Proceedings of the Fall Joint Computer Conference, 1965, pp. 522-525.

[7] Hewlett Packard Company, Application Notes No. 62, 67, and 75.

[8] Kaupp, H.R., "Characteristics of Microstrip Transmission Lines", IEEE Transactions on Electronic Computers, Vol. EC-16, No. 2, April 1967, pp. 185-192.

[9] Lathi, B.P., Random Signals and Communication Theory, Scranton, Pennsylvania: International Textbook Company, 1968, pp. 251-259.

[10] Lathi, B.P., Signals, Systems, and Communication, New York: John Wiley and Sons, Inc., 1965, pp. 127-128 and 483-484.

[11] Millman, Jacob and Taub, Herbert, Pulse, Digital, and Switching Waveforms, New York: McGraw Hill Book Company, Inc., 1965, p. 104.

[12] Muller, Richard S. and Kamins, Theodore I., Device Electronics for Integrated Circuits, New York: John Wiley and Sons, Inc., 1977, pp. 182-183.

[13] Nicolson, A.M., "Forming the Fast Fourier Transform of a Step Response in Time-Domain Metrology", Electron. Lett., Vol. 9, 1973, pp. 317-318.

[14] Oppenheim, Alan V. and Schafer, Ronald W., Digital Signal Processing, Englewood Cliffs, New Jersey: Prentice Hall, Inc., 1975, pp. 27-28, 97-105, and 109-110.

[15] Rabiner, Lawrence R., and Gold, Bernard, Theory and Application of Digital Signal Processing, Englewood Cliffs, New Jersey: Prentice-Hall, Inc., 1975, pp. 50-60.

[16] Taub, Herbert and Schilling, Donald, Digital Integrated Electronics, New York: McGraw Hill Book Company, Inc., 1977, pp. 239-241, 269-270, and 567-573.

[17] Waldmeyer, Jurg, "Fast Fourier Transform for Step-Like Functions: The Synthesis of Three Apparently Different Methods", IEEE Transactions on Instrumentation and Measurement, Vol. IM-29, No. 1, March 1980, pp. 36-39.

[18] Vassel, Gustan N., "Multiple Reflections From RC Loading of Pulse-Signal Transmission Lines", IEEE Transactions on Computers, Vol. C-17, No. 8, August 1968, p. 730.

[19] Wheeler, H.A., "Transmission Line Properties of Parallel Strip Separated by a Dielectric Sheet", IEEE Transactions on Microwave Theory and Techniques, Vol. MTT-13, No. 2, March 1965, pp. 172-185.

[20] Ziemer, R.E. and Tranter, W.H., Principles of Communications, Boston: Houghton Mifflin Company, 1976, pp. 229-330.

Appendix 1

Figures 39 A-D display the TDR voltage steps. The 130 picosecond step is obtained directly from the tunnel diode pulse generator. The slower steps are obtained by installing the Hewlett Packard risetime converters.

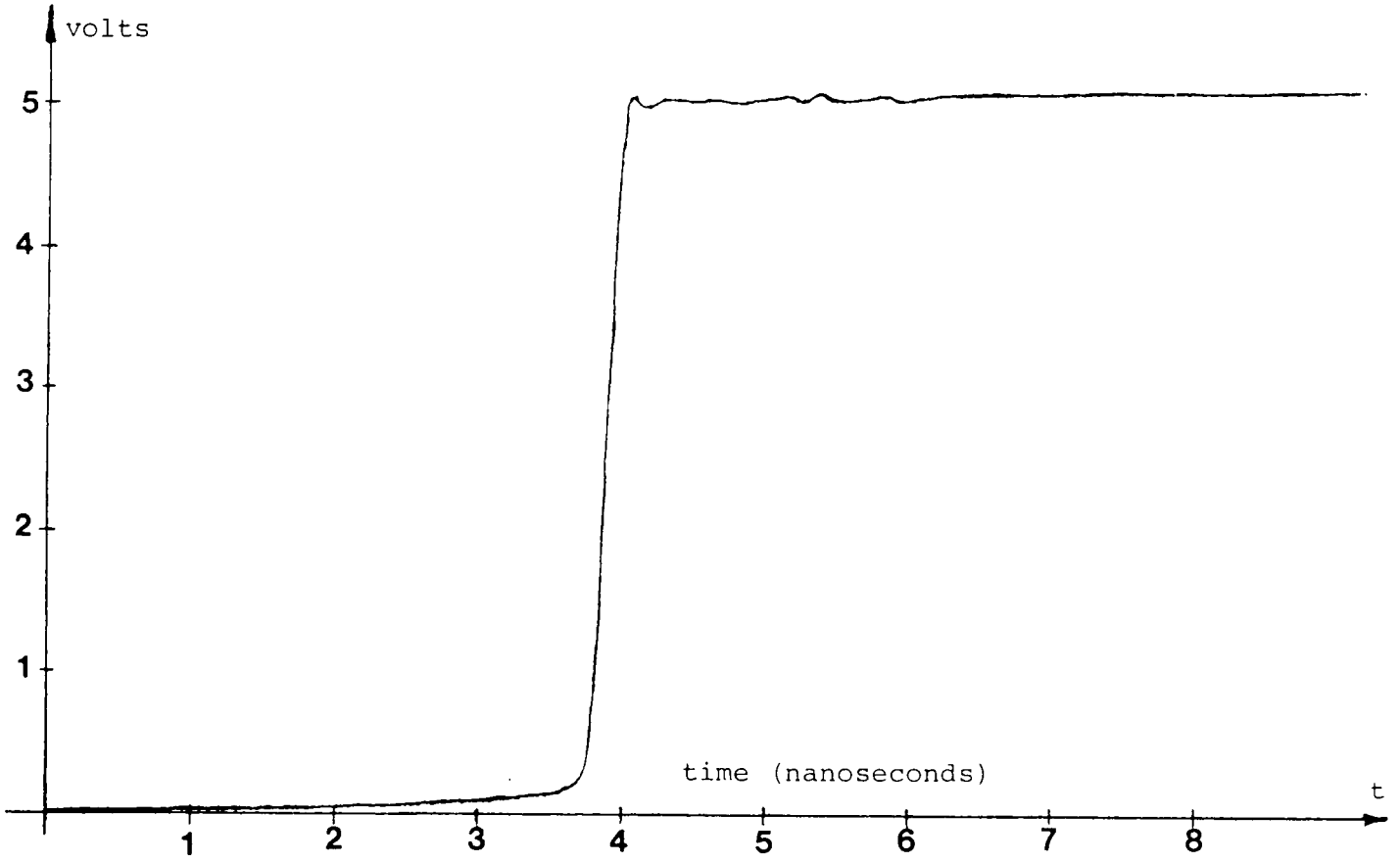

Figure 39A The 130 picosecond step.

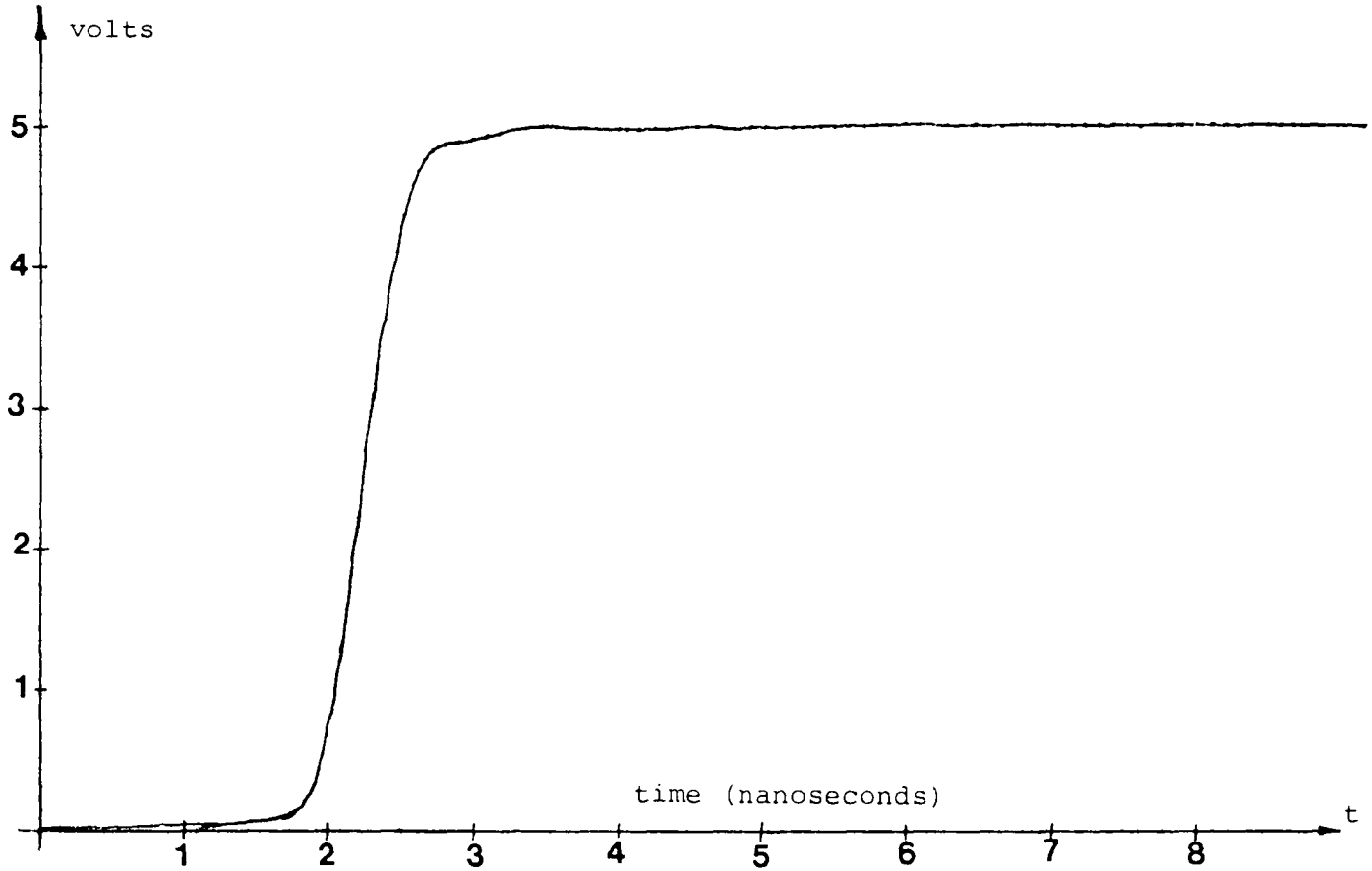

Figure 39B The .5 nanosecond step.

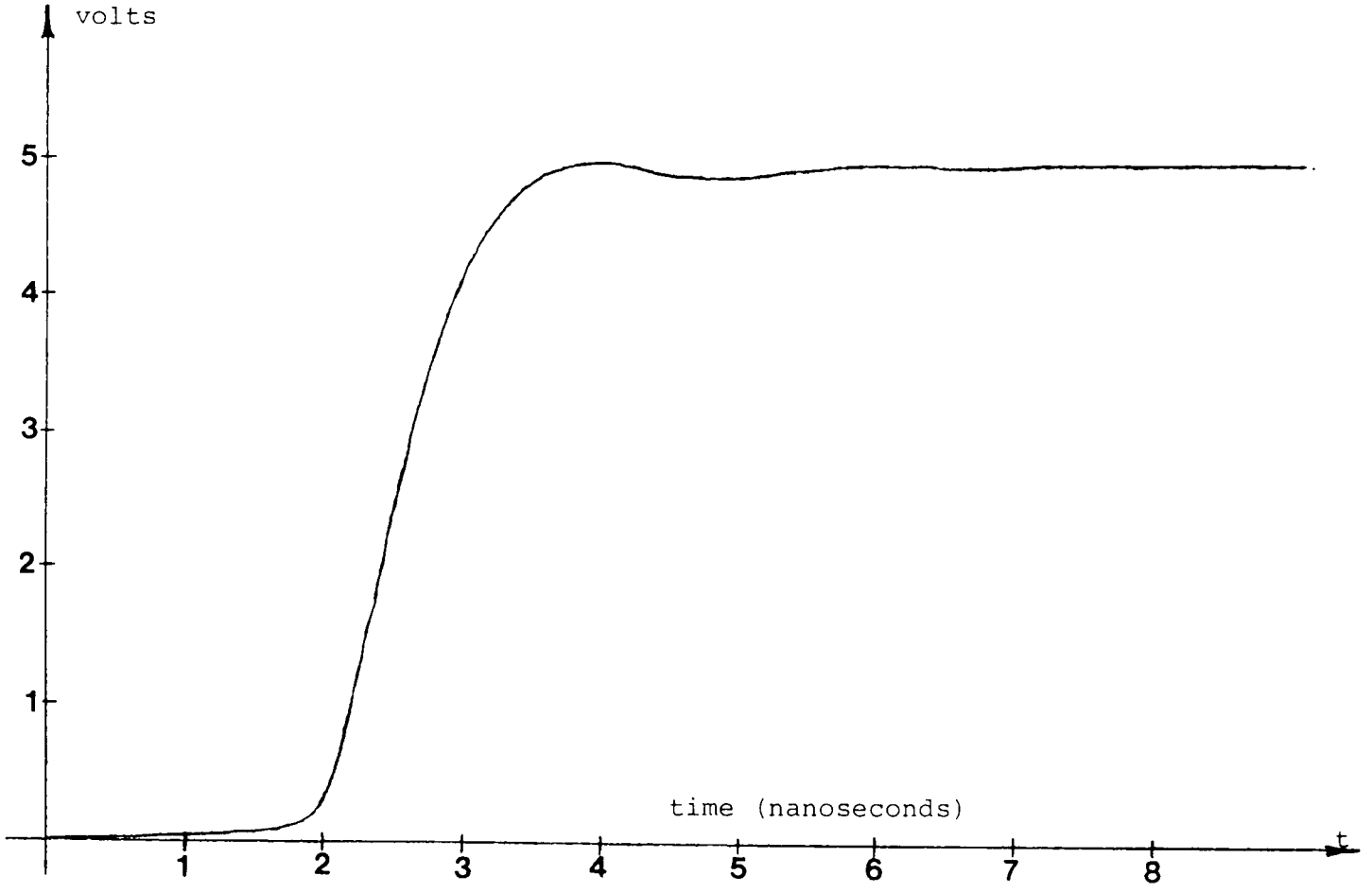

Figure 39C The 1 nanosecond step.

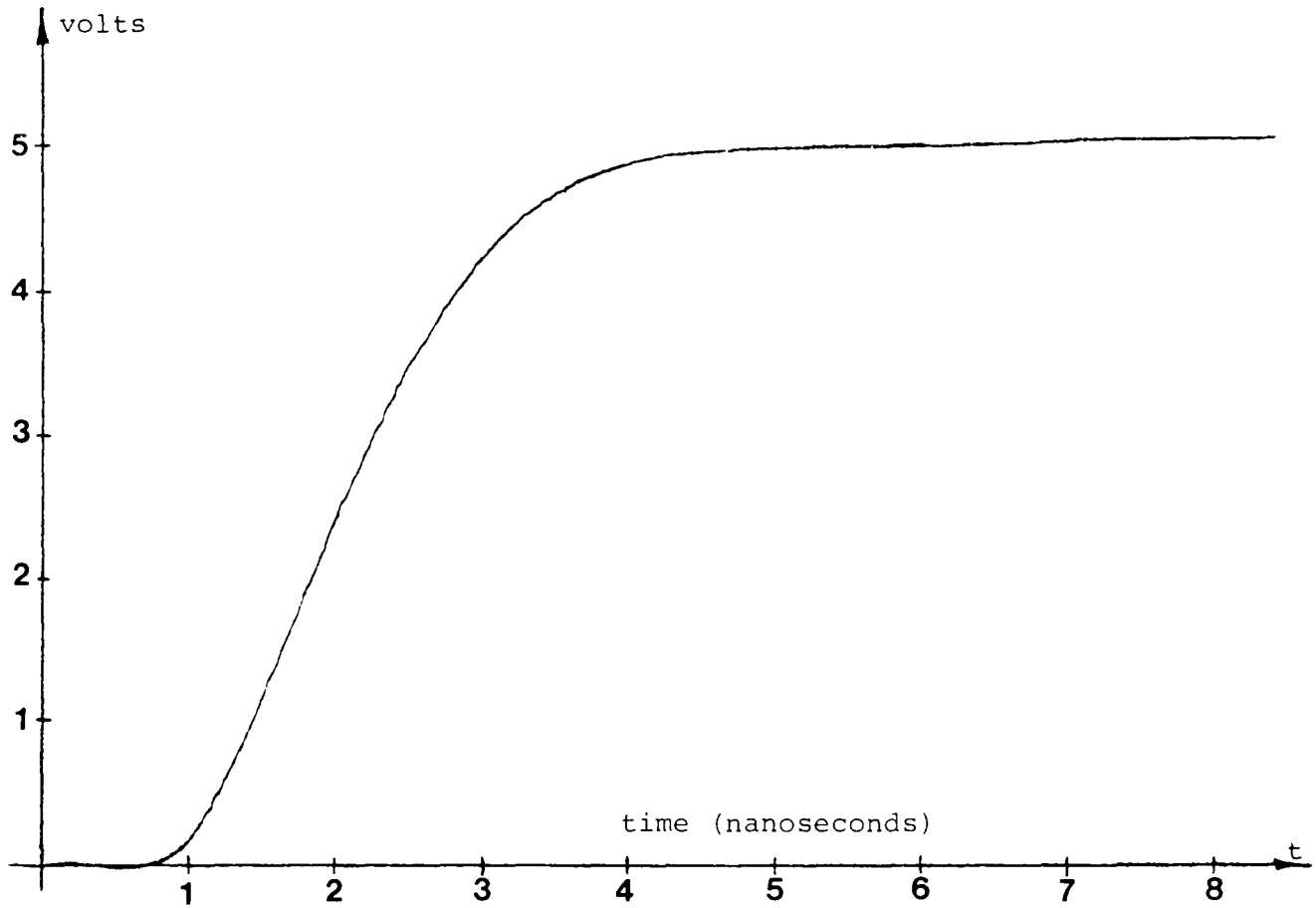

Figure 39D The 2 nanosecond step.

Appendix 2

The situation considered is a coaxial line with characteristic impedance Z_o and propagation time T_D terminated in a capacitor C_L. The TDR transfer function was determined and given in Equation (7) as:

$$H(s) = 1 - e^{-2T_D s} + 2e^{-2T_D s} \cdot \frac{1}{1 + s\tau_L} \qquad (39)$$

where $\tau_L = Z_o C_L$. In this example we use the Laplace Transform and consequently the complex frequency s appears. The analysis could be carried out with the Fourier Transform as well. We have assumed the input steps are of the form

$$E'_{i,\tau}(t) = (1-e^{-t/\tau})\ u(t). \qquad (40)$$

The Laplace Transform of the function in Equation (40) is found in a table to be

$$E'_{i,\tau}(s) = \frac{1}{s(s\tau+1)}. \qquad (41)$$

Next, in correspondence with standard linear system analysis, (see Figure 14) the Laplace Transform of the TDR response is obtained by multiplication of H(s) by $E'_{i,\tau}(s)$. Denoting this as R(s), we find

$$R(s) = \frac{1-e^{-2T_D s}}{s(s\tau+1)} + 2e^{-2T_D s}\left\{\frac{1}{s(1+s\tau_L)(s\tau+1)}\right\}. \quad (42)$$

The expression for R(s) can be simplified to

$$R(s) = \frac{(1-e^{-2T_D s})(1+s\tau_L) + 2\cdot e^{-2T_D s}}{\tau_L \tau (s)(s+\frac{1}{\tau_L})(s+\frac{1}{\tau})}. \quad (43)$$

Equation (43) can be re-expressed in partial fraction form as

$$R(s) = \frac{1}{s(1+s\tau)} + e^{-2T_D s}\left\{\frac{A}{s} + \frac{B}{s+\frac{1}{\tau_L}} + \frac{C}{s+\frac{1}{\tau}}\right\}. \quad (44)$$

The constants A, B, and C can be found from residue evaluation as:

$$A = 1 \quad (45)$$

$$B = \frac{2}{\frac{\tau}{C_L Z_o} - 1} \quad (46)$$

$$C = \frac{1 + C_L Z_o}{C_L Z_o - \tau}. \quad (47)$$

The time domain expression for r(t) can now easily be obtained from Equation (44) as

$$r(t) = (1-e^{-t/\tau})u(t) +$$

$$\left\{ 1 + \frac{2}{\left(\frac{\tau}{C_L Z_o} - 1\right)} \cdot e^{-\frac{(t-2T_D)}{C_L Z_o}} + \right.$$

$$\left. \frac{1 + C_L Z_o}{C_L Z_o - \tau} \cdot e^{-\frac{(t-2T_D)}{\tau}} \right\} u(t-2T_D) \quad (48)$$

which is the result given in Equation (9).

Vita

Joseph Cyril Gabuzda Jr. was born in Lancaster, Pennsylvania on November 14, 1959. He is the son of Joseph and Theresa Gabuzda of Camp Hill, Pennsylvania. He graduated as valedictorian from Camp Hill High School. He graduated with highest honors from Lehigh University in 1980 with a Bachelor of Science degree in Electrical Engineering. He has pursued graduate study at Lehigh under a Lehigh University Distinguished Graduate Fellowship. In addition, he has been employed during the summer periods in the Research Division of AMP Inc., Harrisburg, Pennsylvania. He is a member of the Institute of Electrical and Electronic Engineers and the Society of Physics Students. He is also a member of the Tau Beta Pi and Eta Kappa Nu honorary societies.